Arnold Schwarzenegger
Governor

THE EFFECTS OF AGRICULTURE AND SNOW IMPURITIES ON CLIMATE AND AIR POLLUTION IN CALIFORNIA

PIER PROJECT REPORT

Prepared For:
California Energy Commission
Public Interest Energy Research Program

Prepared By:
Mark Z. Jacobson
Stanford University

November 2007
CEC-500-2007-022

California Climate Change Center
Report Series Number 2007-006

Prepared By:
Mark Z. Jacobson
Department of Civil and Environmental Engineering
Stanford University
Stanford, California 94305-4020

Commission Contract 500-99-013
Commission Work Authorization BOA-144

Prepared For:
Public Interest Energy Research (PIER) Program
California Energy Commission

Beth Chambers
Contract Manager

Kelly Birkinshaw
Program Area Lead
Energy-Related Environmental Research

Laurie ten Hope
Office Manager
Energy System Research

Martha Krebs
Deputy Director
ENERGY RESEARCH & DEVELOPMENT DIVISION

B. B. Blevins
Executive Director

Acknowledgments

This work was funded by California Energy Commission's Public Interest Energy Research Environmental Area (PIER-EA) Program. Thanks go to Guido Franco for providing helpful comments and to William Salas for providing irrigation data.

Please cite this report as follows:

Jacobson, Mark Z. 2007. *The Effects of Agriculture and Snow Impurities on Climate and Air Pollution in California.* California Energy Commission, PIER Energy-Related Environmental Research Program. CEC-500-2007-022.

Preface

The Public Interest Energy Research (PIER) Program supports public interest energy research and development that will help improve the quality of life in California by bringing environmentally safe, affordable, and reliable energy services and products to the marketplace.

The PIER Program, managed by the California Energy Commission (Energy Commission), conducts public interest research, development, and demonstration (RD&D) projects to benefit California's electricity and natural gas ratepayers. The PIER Program strives to conduct the most promising public interest energy research by partnering with RD&D entities, including individuals, businesses, utilities, and public or private research institutions.

PIER funding efforts are focused on the following RD&D program areas:

- Buildings End-Use Energy Efficiency
- Energy-Related Environmental Research
- Energy Systems Integration
- Environmentally Preferred Advanced Generation
- Industrial/Agricultural/Water End-Use Energy Efficiency
- Renewable Energy Technologies
- Transportation

In 2003, the California Energy Commission's Public Interest Energy Research (PIER) Program established the **California Climate Change Center** to document climate change research relevant to the states. This Center is a virtual organization with core research activities at Scripps Institution of Oceanography and the University of California, Berkeley, complemented by efforts at other research institutions. Priority research areas defined in PIER's five-year Climate Change Research Plan are: monitoring, analysis, and modeling of climate; analysis of options to reduce greenhouse gas emissions; assessment of physical impacts and of adaptation strategies; and analysis of the economic consequences of both climate change impacts and the efforts designed to reduce emissions.

The California Climate Change Center Report Series details ongoing Center-sponsored research. As interim project results, the information contained in these reports may change; authors should be contacted for the most recent project results. By providing ready access to this timely research, the Center seeks to inform the public and expand dissemination of climate change information; thereby leveraging collaborative efforts and increasing the benefits of this research to California's citizens, environment, and economy.

The Effects of Agriculture and Snow Impurities on Climate and Air Pollution in California is the final report for the Scoping Study on the Effects of Black Carbon on the Reflectivity of Snow and Agricultural Irrigation on Surface Temperatures project (contract 500-99-013, work authorization BOA-144) conducted by Stanford University.

For more information on the PIER Program, please visit the Energy Commission's website www.energy.ca.gov/pier/ or contract the Energy Commission at (916) 654-5164.

Table of Contents

List of Figures

List of Tables

Abstract

This paper discusses the effects of agriculture and snow impurities on California climate and air pollution. High-resolution data were used with the GATOR-GCMOM model to examine these issues. Results suggest that irrigation alone increased nighttime temperatures but decreased daytime temperatures more, causing a net cooling in California of about 0.025 K (0.045°F) during August 2006. The conversion of native land in the 1800s to agriculture increased the albedo of the northern and middle San Joaquin Valley and decreased that of the southernmost valley, causing a net cooling due to irrigation plus albedo change of 0.03 K (0.054°F). Maximum local decreases were 0.7 K (1.26°F), occurring in the San Joaquin Valley. Irrigation also increased soil moisture, relative humidity, cloud optical depth, and drizzle and decreased wind speeds. Irrigation further increased low-solubility gases, such as carbon monoxide and methane but decreased soluble gases, such as nitric acid and sulfur dioxide, and slightly decreased ozone. Absorption of sunlight by black carbon and soildust in snow during February reduced land (snow plus nonsnow) albedo by 0.3 percent, reduced land-averaged snow depth by 0.5 percent, increased ground temperatures by 0.11 K (1.98°F), and increased soil moisture by 0.07 percent. Because snow impurities hasten meltwater release and decrease soil water, reducing particle emissions can benefit water supply.

Keywords: Agriculture, snow impurities, California climate, air pollution, GATOR-GCMOM model, albedo, irrigation, black carbon, soil dust

Executive Summary

Introduction

The effects of agriculture and snow impurities on California's climate and air quality are important. Observed global warming to date, approximately 1.35°F–1.44°F above the global average recorded since 1850, is attributed to greenhouse gases and absorbing aerosol particles. This temperature rise is simultaneously offset by cooling due to reflective aerosol particles. Regional land use changes (such as conversion to agriculture) and increased pollutants in snow can also affect regional temperatures, weather, air pollution, and water supply.

Purpose

The project's purpose was to examine and quantify the short-term effects of agriculture and snow impurities on California climate and air quality.

Project Objective

This project's objective was to conduct baseline and sensitivity numerical experiments to quantify the effects of agriculture and snow impurities on California's climate and air quality. The researcher ran simulations for August 2006 to examine the effects of agriculture and February 1999 to examine the effects of snow impurities. The model used was GATOR-GCMOM—a nested, global-through-urban-scale gas, aerosol, transport, radiation, general circulation, mesoscale, and ocean model. Emission data used for the model were highly resolved in space and time. The model treated the formation of clouds and precipitation from aerosol particles from physical principles and radiative transfer through clouds, aerosol particles, gases, and snow.

To study the effects of agriculture, the researcher ran separate simulations examining the effects of (1) irrigation alone, and (2) irrigation plus albedo (the fraction of light reflected by a surface) change due to agriculture. To study the effects of impurities, the researcher accounted for absorption and scattering by black carbon and soildust inclusions in snow. These impurities entered snow by wet and dry deposition following long-range and local transport. However, the contributions of pollution from Asia versus California were not separately quantified.

Project Outcomes

Results from the simulations helped to clarify some previously unanswered questions about the effects of agriculture on California climate and air quality. First, conversion to agriculture since the 1800s may have resulted in an albedo *increase* of the northern and middle San Joaquin Valley, but an albedo *decrease* of the southern valley. This result makes sense considering that, in the 1800s, the northern and middle valley was mostly low-albedo rangeland and marshland and the southern valley below Lake Tulare was mostly high-albedo desert. The result also suggests that, when only albedo is considered, agriculture should slightly cool near-surface air temperatures during the day. Irrigation should also cool air during the day but warm it at night.

From the simulations, it was found that irrigation alone decreased near-surface air temperatures by about 0.045°F and irrigation plus albedo changes decreased temperatures by about 0.054°F in the monthly average over all irrigated-plus-nonirrigated land. Nighttime temperatures increased, while daytime temperatures decreased to a greater extent. Maximum local decreases in August temperatures were about 1.26°F, occurring in the San Joaquin Valley. Irrigation increased soil moisture by an average over land of about 6 percent, the relative humidity by about 0.4 percent, cloud optical depth by about 8 percent, cloud fraction (the amount of cloud in the sky) by about 5 percent, and drizzle by about 7 percent.

By increasing stability and reducing near-surface wind speeds, agriculture increased the mixing ratios of low-solubility, slowly reacting gases, such as carbon monoxide (CO) and methane (CH_4). By increasing cloudiness and wet removal (that is, removal by precipitation), agriculture decreased the mixing ratios of soluble gases, such as nitric acid (HNO_3) and sulfur dioxide (SO_2). Further, agriculture shifted the mass of most chemical components from aerosols to clouds and precipitation.

With respect to the snow simulations, absorption of solar radiation by black carbon and soildust in snow reduced snow-plus-nonsnow covered land albedo during February by about 0.3 percent, reduced land-averaged snow depth by about 0.5 percent, increased ground temperatures over land by about 0.198°F, increased soil moisture by about 0.07 percent, and increased the relative humidity by about 0.04 percent. Impurities in snow were found to decrease available water by (1) increasing sublimation (that is, going from a solid to a vapor without becoming a liquid), and (2) hastening meltwater release by increasing soil moisture.

Conclusions

Since agriculture may have caused a net increase in albedo and a net cooling of the San Joaquin Valley, the valley's observed historic warming may be due to anthropogenic pollutants rather than albedo change. Recently, the net effect of scattering-plus-absorbing aerosol particles was shown to cool the valley. As such, observed warming may be attributable to greenhouse gases less the net cooling effect of aerosol particles.

Irrigation from agriculture also affected clouds and moisture, reducing the intensity of total and ultraviolet sunlight reaching the ground.

Feedbacks of irrigation to air pollution depend on whether irrigation enhances rainfall. When it does, pollution decreases, due to enhanced pollution removal by wet deposition. When irrigation does not enhance rainfall, irrigation's main effect is to stabilize the air by cooling the ground. Enhanced stability reduces vertical turbulence and horizontal wind speeds, thereby inhibiting certain air pollutants from mixing vertically and horizontally; increasing their concentrations.

The addition of absorbing impurities to snow warms it, hastening meltwater release and increasing sublimation (which decreases the water available for runoff). Although the effects of impurities on snow melting and sublimation should be greater in April than in February (due to warmer temperatures and greater solar radiation in April), snow area in April is much smaller

than in February, so newly deposited impurities from Asia may have a lesser aggregate impact on snowmelt (by the time they arrive in April) than local impurities, which are deposited over a larger snow area during a period starting long before April.

Recommendations

The numerical model results here are a step in the long process of trying to understand better the effects of land use and pollution changes on climate and air quality. Whereas, the signs of the changes due to agriculture and impurities in snow found here appear robust, the magnitudes are more uncertain. Such uncertainty can be reduced by improving model resolution; initialization; treatment of physical, chemical, and dynamical processes; and input datasets. Additional measurements of impurities in snow and meteorology at different distances from irrigated fields could also increase understanding of the effects examined here.

The results of this study imply that irrigation from agriculture can enhance air pollution when clouds and rain are not imminent or present, and for insoluble gases when they are. When clouds and rain are imminent or present, irrigation increases the wet removal of soluble gas and aerosol pollutants by increasing precipitation. Although increasing wet removal of pollutants improves air quality, such removal increases the pollution content of runoff. Further studies are necessary to examine the effect of the increased pollutant content of runoff due to irrigation. This study did not examine changes in emissions due to agriculture practices, such as disking, planting, fertilizing, harvesting, and transporting crops, so the author can only draw conclusions about the effects of irrigation and albedo change.

This study also demonstrated that absorbing air pollution particles affect snowmelt, snow albedo, and ground temperatures—even in February. As such, efforts to reduce particle emissions, including both local and Asian emissions, will help to alleviate slightly the effect of climate change on early release of melt water.

Benefits to California

This study examined effects in California and parts of Nevada. It provided answers to several previously unanswered questions about the effects of agriculture and snow impurities on California climate and air pollution and provided recommendations of methods to ameliorate the effects. If implemented, the recommendations could have collateral benefits. For example, reducing absorbing particle (such as soot) emissions, improves human health as well as reducing impacts on snowmelt. Similarly, reducing evaporation during irrigation not only reduces air pollution in rain-free areas but reduces the pollutant content of rainwater and increases water available to a growing population. Because irrigation may increase air pollution removal when clouds and rain are imminent or present, irrigation may provide an air quality benefit in some situations.

1.0 Introduction

Climate and air quality in California are undergoing changes that are expected to increase in the future. In order to focus regulation correctly, it is important to attribute accurately the changes to their causes. Whereas data analysis shows correlation between a hypothesized cause and an effect, only numerical modeling can attribute an effect to a specific cause. The purpose of this study was to use a numerical model to examine the effects of agriculture (irrigation and albedo change) and of pollutants in snow on California climate and air quality. First, previous work on these two topics is discussed.

1.1. Effects of Agriculture

The replacement of virgin landscape with agriculture results in several sources of climate change: an increase in irrigation, a change in surface albedo, a change in the storage of carbon in the land, and the emissions of climate- and air-pollution-relevant gases and particles. Such emissions occur during the production and use of fertilizers and during cultivation, harvesting, and transport of agricultural food products. This paper examines only the effects of irrigation and albedo change on regional climate and air quality.

Irrigation affects soil moisture, which affects ground temperatures, vertical temperature profiles, and evaporation rates. Temperature profiles affect boundary layer depths, air pressures, wind speed, and wind direction. Evaporation affects the relative humidity, cloud formation, and precipitation. The effects of soil moisture on planetary boundary layer depth circulation patterns, and/or clouds have been studied by Zhang and Anthes (1982); Ookouchi et al. (1984); Mahfouf et al. (1987); Lanicci et al. (1987); Cuenca et al. (1996); Emori (1998); Jacobson (1999); Fennessy and Shukla (1999); and Martilli (2002); among others. The sensitivity of global meteorology to soil moisture variations has been studied by Walker and Rowntree (1977); Rind (1982); Mintz (1984); and Schar et al. (1999), among others.

On an urban scale, Jacobson (1999) examined the effect of soil moisture on air pollution particles and gases, temperatures, and winds in Los Angeles. The study did not consider feedbacks of soil moisture to clouds and precipitation. In the absence of cloud feedbacks, decreasing soil moisture increased temperatures between the surface and 600 hectopascal (hPa), increased near-surface wind speeds, but decreased near-surface pollutant concentrations over two days. Increasing soil moisture had the opposite effect. Slower wind speeds, associated with high soil moisture contents, delayed times of peak ozone mixing ratios in the eastern Los Angeles basin. Faster wind speeds, associated with low soil moisture contents, advanced times of peak mixing ratios. High soil moisture resulted in thinner boundary layer depths, increasing average near-surface primary pollutant concentrations. Low soil moisture resulted in thicker boundary layer depths, decreasing average concentrations.

Barnston and Schickedanz (1984) concluded from data that irrigation from 1931–1970 over the southern Great Plains of the United States was correlated with a decrease in surface temperature and an increase in precipitation. In a modeling study, Segal et al. (1998) found a continental-averaged increase in average rainfall due to irrigation in North America over the last 100 years. Moore and Rojstaczer (2001), however, suggested through data analysis that

irrigation-induced rainfall over the Great Plains of the United States between 1950 and 1997 was minor in comparison with natural factors affecting rainfall. They attributed the difference between results of Barnston and Schickedanz (1984) and their own study in part to general climate change, rather than irrigation change.

Christy et al. (2006) analyzed data and suggested that temperatures in the San Joaquin Valley of California increased at a rate of 0.07°C per decade from 1910–2003, whereas temperatures in the Sierra Nevada Mountains decreased at -0.02°C per decade. They attributed the difference to a decrease in the albedo of the valley relative to the mountains caused by irrigation during that period that resulted in greener vegetation. Snyder et al. (2006), on the other hand, who compared results from four regional climate models applied to the western United States, found that irrigation combined with landcover change decreased surface temperature in three out of four models tested. Similarly, Adegoke et al. (2003) found that combining increases in irrigation with land-use changes cooled the ground. Lobell et al. (2006) examined the effect of changes in irrigation, tillage, and crop productivity on global temperatures. They found that irrigation resulted in a global cooling; whereas increasing tillage caused a decrease in surface albedo and a slight global warming. The decrease in temperature due to greater irrigation outweighed the increase in temperature due to higher albedo. Boucher et al. (2004) found that increasing irrigation without a change in land use cooled the ground.

This study examined the effects of irrigation and albedo change due to agriculture on California climate and air quality.

1.2. Effects of Soot and Soildust

Fossil-fuel soot consists primarily of black carbon (BC), organic matter (OM), and lesser amounts of sulfate and other material. Black carbon warms the air directly by absorbing solar radiation, converting the solar radiation into internal energy (raising the temperature of the soot), and emitting, at the higher temperature, thermal-infrared radiation, which is absorbed selectively by air molecules. The energized air molecules, which have long lifetimes, are transported to the large scale, including the global scale. The soot particles, which are removed within days to weeks by rainout, washout, and dry deposition, do not travel so far as do the air molecules, but can travel hemispherically or globally under the right conditions.

Because soot particles absorb solar radiation, they prevent that radiation from reaching the ground, thereby cooling the ground immediately below them during the day. During the day and night, BC absorbs the Earth's thermal-infrared radiation, a portion of which is redirected back to the ground, warming the ground. In sum, soot particles create three major types of vertical temperature gradients: (1) a daytime gradient in the immediate presence of soot, where the atmosphere warms and the ground cools; (2) a nighttime gradient in the immediate presence of soot, where the atmosphere warms and the ground warms; and (3) a large-scale day- and nighttime gradient in the absence of soot but in the presence of advected air heated by soot, where the atmosphere warms and the ground temperature does not change. In only the first case, which covers only a portion of the globe and only during the day, does soot cool the

ground. These three types of vertical temperature gradients set in motion feedbacks to meteorology, clouds, other aerosol components, and radiation that affect temperatures further.

When BC deposits to a surface, such as snow, it warms the surface by absorbing solar radiation. The heating melts snow, reducing snow depth and reflectivity. Soildust is a weaker solar absorber but is often present in greater concentrations than is black carbon. When soildust deposits to snow, it also absorbs sunlight, melting snow, reducing snow depth and reflectivity.

Several studies have reported measurements of black carbon in snow (e.g., Warren 1982, 1984; Clarke and Noone 1985; Chylek et al. 1987; Noone and Clarke 1988; Warren and Clarke 1990; Grenfell et al. 1994, 2002). Other studies have modeled the albedo of snow containing BC inclusions (e.g., Warren and Wiscombe 1980, 1985; Chylek et al. 1983; Warren 1984; Aoki et al. 2000), the albedo of sea ice containing BC inclusions (Light et al. 1998), and the optical properties of ice or snow containing other inclusions (e.g., Higuchi and Nagoshi 1977; Gribbon 1979; Clark and Lucey 1984; Woo and Dubreuil 1985; Podgorny and Grenfell 1996). Warren and Wiscombe (1980), for example, found that a concentration of 15 nanograms per gram (ng/g) of soot in snow might reduce the albedo of snow by about 1%.

A third, recent set of studies has examined the effect on global climate of albedo changes due to soot in snow. Hansen and Nazarenko (2003) calculated, by prescribing changes in surface albedos, that BC absorption in snow and sea ice, alone, might cause 0.17 K of the observed global warming to date. Jacobson (2004) performed global simulations in which the time-dependent spectral albedos and emissivities over snow and sea ice were predicted with a radiative transfer solution, rather than prescribed. The model treated the cycling of size-resolved black-carbon-plus-organic-matter (BC+OM) between emission and removal by dry deposition and precipitation to snow, sea ice, and other surfaces. Particles entered size-resolved clouds and precipitation by nucleation scavenging and aerosol-hydrometeor coagulation. Precipitation brought BC to the surface, where internally and externally mixed BC in snow and sea ice affected albedo and emissivity through radiative transfer. The 10-year averaged incremental warming due to absorption of fossil-fuel-plus-biofuel soot in snow and sea ice was +0.06 K with a modeled range of +0.03 to +0.11 K. BC was calculated to reduce snow and sea ice albedo by about 0.4% in the global average and 1% in the Northern Hemisphere. The globally averaged modeled BC concentration in snow and sea ice from all sources was about 5 ng/g; that in rainfall was about 22 ng/g. About 98% of BC removal from the atmosphere was due to precipitation; the rest, to dry deposition. Hansen et al. (2005) reestimated the effect of snow albedo changes due to BC on surface temperatures as +0.065 K. Flanner et al. (2006) estimate the climate response of biomass-plus-biofuel-plus-fossil-fuel BC as +0.1 K (with low forest fire emissions) to +0.15 K (high forest fire emissions). With 80% of the BC in the low-fire case being due to fossil-plus biofuels, the resulting warming due to these sources was about +0.08 K.

Black carbon and soildust in snow in the Sierra Nevada Mountains can originate locally or from Asia. Some measurement and modeling studies have shown that pollution outflow from Asia is maximum around April (e.g., Goldstein et al. 2004; Park et al. 2005). Asian aerosol particles appear at sea level in the United States primarily during April, but aerosol mass at elevated mountain sites in the western United States may be present all year (VanCuren et al. 2005).

VanCuren and Cahill (2002) similarly found that Asian pollution in North America peaked in spring at 500–3000 meters (m) above sea level in concentrations between 0.2 and 5 micrograms per square meter ($\mu g/m^3$), and Roberts et al. (2006) found Asian aerosols in stratified layers between 500 and 7500 m above sea level. The composition of Asian particle pollution has been estimated in one study as 30% mineral, 28% organic compounds, 4% black carbon, 10% sulfate, < 5% nitrate and < 1% sea salt (Van Curen 2003). Asian dust is thought to comprise about 10%–15% of fine particle mass at elevated sites in the Western United States (Liu et al. 2003).

This study examined the effects of black carbon and soildust absorption in snow on ground temperatures, soil moisture, snow depth, reflectivity, relative humidity, and other parameters. The study accounted for the long-range and local transport of soildust and black carbon but did not isolate which contributions are long-range and which are local. The simulations were carried out for February 1999. Although more black carbon and soildust travel from Asia to North America in April than in February, snow depths and snow areas in California are greater in February than in April. For example, the climatological mean snow depth at Mammoth Lakes is 30 inches in February and 9 inches in April. That at Sagehen Creek is 41 inches in February and 21 inches in April. That at Yosemite is 9 inches in February and 2 inches in April. That at Sierra City is 21.3 inches in February and 7.6 inches in April (Western Regional Climate Center 2006). As such, soildust and black carbon coming from Asia in April fall over a smaller surface area of snow than does local soildust and black carbon in February. On the other hand, incident solar radiation and temperatures are greater in April than in February, so the same level of impurities in snow should cause more melting per unit area of snow in April than in February. Because the simulations here were carried out in February, they may underestimate the effect of impurities on the melt rate.

2.0 Model Description

The model used for this study was GATOR-GCMOM, a parallelized and one-way-nested global-through-urban scale Gas, Aerosol, Transport, Radiation, General Circulation, Mesoscale, and Ocean Model (Jacobson 1997a, 1997b; 2001a, 2001b; 2002a; 2004; 2006). The model treated time-dependent gas, aerosol, cloud, radiative, dynamical, ocean, and transport processes.

2.1. Atmospheric Dynamical and Transport Processes

On the global scale, the model solved the hydrostatic momentum equation and the thermodynamic energy equation with the potential-enstrophy, mass, and energy-conserving scheme of Arakawa and Lamb (1981). In nested regional domains, the solution scheme conserved enstrophy, mass, and kinetic energy (Lu and Turco 1995). Dynamical schemes on all domains used spherical and sigma-pressure coordinates in the horizontal and vertical, respectively. Transport of gases (including water vapor) and aerosol particles was solved with the scheme of Walcek and Aleksic (1998) using modeled online winds and vertical diffusion coefficients, determined by the 2.5 order turbulence closure of Mellor and Yamada (1982).

2.2. Gas Processes

Gas processes included emission, photochemistry, advection, turbulence, cloud convection of gases, nucleation, washout, dry deposition, and condensation onto (and dissolution into) aerosol particles, clouds, and precipitation. Gases affected solar and thermal-infrared radiation, aerosol formation, and cloud evolution, all of which fed back to meteorology. Gas photochemistry was solved with SMVGEAR II (Jacobson 1998). The chemical mechanism for this study included 143 gases, 282 kinetic reactions, and 36 photolysis reactions.

2.3. Aerosol Processes

For the present application, aerosol processes were treated with a single size distribution consisting of 12 size bins ranging from 0.002 to 50 micrometers (μm) in diameter, and 16 aerosol components per bin (Table 1). The model is generalized though, so that any number of discrete, interacting aerosol size distributions can be treated and used for cloud development (Jacobson 2003). The aerosol size bin structure was the moving-center structure, whereby bin edges were fixed but bin centers moved in diameter space due to changes in particle size (Jacobson, 1997a). Parameters treated prognostically in each size bin included particle number concentration and individual component mole concentration. Single-particle volume was calculated assuming particles contained a solution and nonsolution component, as in Jacobson (2002b), which also describes most numerical techniques used for solving aerosol physical and chemical processes.

Table 1. Aerosol and hydrometeor size distributions treated in the model and the chemical constituents present in each size bin of each size distribution

Aerosol Internally Mixed (IM)	Cloud / Precipitation Liquid	Cloud / Precipitation Ice	Cloud / Precipitation Graupel
Number	Number	Number	Number
BC	BC	BC	BC
POM	POM	POM	POM
SOM	SOM	SOM	SOM
H_2O(aq)-hydrated	H_2O(aq)-hydrated	H_2O(aq)-hydrated	H_2O(aq)-hydrated
H_2SO_4(aq)	H_2SO_4(aq)	H_2SO_4(aq)	H_2SO_4(aq)
HSO_4^-	HSO_4^-	HSO_4^-	HSO_4^-
SO_4^{2-}	SO_4^{2-}	SO_4^{2-}	SO_4^{2-}
NO_3^-	NO_3^-	NO_3^-	NO_3^-
Cl^-	Cl^-	Cl^-	Cl^-
H^+	H^+	H^+	H^+
NH_4^+	NH_4^+	NH_4^+	NH_4^+
NH_4NO_3(s)	NH_4NO_3(s)	NH_4NO_3(s)	NH_4NO_3(s)
$(NH4)_2SO_4$(s)	$(NH4)_2SO_4$(s)	$(NH4)_2SO_4$(s)	$(NH4)_2SO_4$(s)
Na^+ (K^+,Mg^{2+},Ca^{2+})	Na^+ (K^+,Mg^{2+},Ca^{2+})	Na^+ (K^+,Mg^{2+},Ca^{2+})	Na^+ (K^+,Mg^{2+},Ca^{2+})
Soildust	Soildust	Soildust	Soildust
Pollen/spores/bact.	Pollen/spores/bact.	Pollen/spores/bact.	Pollen/spores/bact.
	H_2O(aq)-condensed	H_2O(s)	H_2O(s)

POM is primary organic matter; SOM is secondary organic matter. H_2O(aq)-hydrated is liquid water hydrated to dissolved ions and undissociated molecules in solution. H_2O(aq)-condensed is water that condensed to form liquid hydrometeors. Condensed and hydrated water existed in the same particles so that, if condensed water evaporated, the core material, including its hydrated water, remained. H_2O(s) was either water that froze from the liquid phase or that directly deposited from the gas phase as ice. Emitted particles included fossil-fuel soot (BC, POM, H_2SO_4(aq), HSO_4^-, SO_4^{2-}), sea spray (H_2O, Na^+, K^+, Mg^{2+}, Ca^{2+}, Cl^-, NO_3^-, H_2SO_4(aq), HSO_4^-, and SO_4^{2-}), biomass and biofuel burning (same chemicals as sea spray plus BC, POM), soildust, pollen, spores, and bacteria. For sea spray and biomass/biofuel burning, K^+, Mg^{2+}, Ca^{2+} were treated as equivalent Na^+. Homogenously nucleated species (H_2O, H_2SO_4(aq), HSO_4^-, SO_4^{2-}. NH_4^+) entered the internally mixed distribution. Condensing gases on all distributions included H_2SO_4 and SOM. Gases dissolving in all distributions included HNO_3, HCl, and NH_3. The liquid water content and H^+ of each bin were determined as a function of the relative humidity and ion composition from equilibrium calculations. All distributions were affected by self-coagulation loss to larger sizes and heterocoagulation loss to other distributions (except the internally mixed distribution, which had no heterocoagulation loss).

Size-dependent aerosol processes included emission, homogeneous nucleation, condensation, dissolution, aerosol-aerosol coagulation, aerosol-cloud/ice/graupel coagulation, equilibrium hydration of liquid water, internal-particle chemical equilibrium, irreversible aqueous chemistry, evaporation of cloud drops to aerosol-particles, transport, sedimentation, dry deposition, rainout, and washout. Aerosol particles affected solar and thermal-IR radiation, cloud evolution, gas concentration, and surface albedo, all of which fed back to meteorology.

Homogeneous nucleation and condensation of sulfuric acid were solved simultaneously between the gas phase and all size bins with a mass-conserving, noniterative, and unconditionally stable scheme (Jacobson 2002b) that also solved condensation of organic gases onto size-resolved aerosol particles. The model further treated nonequilibrium dissolutional growth of inorganics (e.g., ammonia [NH_3], nitric acid [HNO_3], hydrogen chloride [HCl]) and soluble organics to all size bins with a mass-conserving nonequilibrium growth solver, PNG-EQUISOLV II (Jacobson 2005a), where PNG is Predictor of Nonequilibrium Growth. EQUISOLV II is a chemical equilibrium solver that determines aerosol liquid water content, pH,

and ion distributions following nonequilibrium growth. Aerosol-aerosol coagulation was solved among all size bins and components and among total particles in each bin with a volume-conserving, noniterative, algorithm (Jacobson 2002b). Coagulation kernels included those for Brownian motion, Brownian diffusion enhancement, van der Waals forces, viscous forces, fractal geometry of soot aggregates, turbulent shear, turbulent inertial motion, and gravitational settling.

2.4. Regional-Scale Gas-Aerosol-Cloud-Turbulence Interactions

Cloud thermodynamics and microphysics in the regional domain were treated explicitly (Jacobson et al. 2007). The cloud module included algorithms that treated the three-dimensional (3-D) time-dependent evolution and movement of aerosol-containing size- and composition-resolved clouds and precipitation. Water vapor and size- and composition-resolved aerosol particles were transported using predicted horizontal and vertical velocities. When the partial pressure of water vapor exceeded the saturation vapor pressure over liquid water or ice on an aerosol particle or pre-existing hydrometeor-particle surface, water vapor condensed or deposited on the particle. The saturation vapor pressure was affected by the Kelvin effect and Raoult's law, both of which were calculated from aerosol and hydrometeor composition. Thus, changes in, for example, surface tension due to organics and inorganics affected the activation properties of aerosol particles. The numerical solution for hydrometeor growth accounted for water vapor condensation and deposition onto all activated size-resolved aerosol particles and pre-existing size-resolved hydrometeor simultaneously. The numerical scheme was unconditionally stable, noniterative, positive-definite, and mole conserving.

Following the condensation/deposition calculation, liquid drops and ice crystals were partitioned from a single size-resolved aerosol distribution into separate liquid and ice hydrometeor size distributions, where each discrete size bin contained all the chemical components of the underlying CCN aerosol particles. Table 1 shows the chemical makeup of these two distributions. A third discretized hydrometeor distribution—graupel—was also tracked. This distribution formed upon heterocoagulation of the liquid water and ice hydrometeor distributions, contact freezing of aerosol particles with the liquid distribution, heterogeneous-homogeneous freezing of the liquid distribution, and evaporative freezing of the liquid distribution. The graupel distribution also contained all the chemical components from the aerosol and other hydrometeor distributions (Table 1).

Following the partitioning of aerosol particles to liquid drops and ice crystals, the size-resolved cloud processes treated in the model included the following:

- hydrometeor-hydrometeor coagulation (liquid-liquid, liquid-ice, liquid-graupel, ice-ice, ice-graupel, and graupel-graupel)
- aerosol-hydrometeor coagulation
- large liquid drop breakup
- settling to the layer below (or precipitation from the lowest layer to the surface)
- evaporative cooling during drop settling

- evaporative freezing (freezing during drop cooling)
- heterogeneous-homogeneous freezing
- contact freezing
- melting
- evaporation
- sublimation release of aerosol cores upon evaporation/sublimation
- coagulation of hydrometeors with interstitial aerosols
- irreversible aqueous chemistry
- gas washout
- lightning generation from size-resolved coagulation among ice hydrometeors.

The kernel for all cloud coagulation interactions and aerosol-cloud coagulation interactions included a coalescence efficiency and collision kernels for Brownian motion, Brownian diffusion enhancement, turbulent inertial motion, turbulent shear, settling, thermophoresis, diffusiophoresis, and charge. Numerical techniques used for these processes are given in Jacobson (2003).

During the microphysical calculations, changes in energy due to condensation, evaporation, deposition, sublimation, freezing, and melting were included as diabatic heating terms in the thermodynamic energy equation; energy was conserved exactly due to cloud formation and decay. Similarly, total water (water vapor, size-resolved aerosol water, size-resolved cloud water, soil water, and ocean water) was conserved exactly.

Following the cloud- and aerosol microphysical calculations each time step, size-resolved aerosol particles and hydrometeors particles (if they existed) in each grid cell were transported by the horizontal and vertical winds and turbulence. Thus, three-dimensional size-resolved clouds (such as stratus, cumulus, cumulonimbus, and cirrus) formed, moved, and dissipated in the model.

Aerosol particles of different size were removed by size-resolved clouds and precipitation through two mechanisms: nucleation scavenging and aerosol-hydrometeor coagulation. Both processes were size-resolved with respect to both aerosol particles and hydrometeor particles.

2.5. Radiative Processes

Radiative processes include ultraviolet (UV), visible, solar-infrared (IR), and thermal-IR interactions with gases, size/composition-resolved aerosols, and size/composition-resolved hydrometeor particles. Radiative transfer was solved with the scheme of Toon et al. (1989). Calculations were performed for > 600 wavelengths/probability intervals and affected photolysis and heating. Gas absorption coefficients in the solar-IR and thermal-IR were calculated for water (H_2O), carbon dioxide (CO_2), methane (CH_4). Carbon monoxide (CO), ozone (O_3), oxygen (O_2), nitrous oxide (N_2O), methyl chloride (CH_3Cl), trichlorofluoromethane

($CFCl_3$), dichlorodifluoromethane (CF_2Cl_2), and carbon tetrachloride (CCl_4) as in Jacobson (2005b). Aerosol-particle optical properties were calculated assuming that BC (if present in a size bin) comprised a particle's core and all other material coated the core. Shell real and imaginary refractive indices for a given particle size and wavelength were obtained by calculating the solution-phase refractive index, calculating refractive indices of non-solution, non-BC species, and volume averaging solution and nonsolution refractive indices. Core and shell refractive indices were used in a core-shell Mie-theory calculation (Toon and Ackerman 1981). Cloud liquid, ice, and graupel optical properties for each hydrometeor size and radiation wavelength were also determined from Mie calculations by assuming cloud drops and ice crystals contained a BC core surrounded by a water shell. The surface albedos of snow, sea ice, and water (ocean and lake) were wavelength-dependent and predicted by (rather than specified in) the model (Jacobson 2004).

2.6. Ocean Surfaces

Ocean mixed-layer velocities, energy transport, and mass transport were calculated with a gridded two-dimensional (2-D) potential enstrophy-, kinetic energy-, and mass-conserving shallow-water equation module, forced by wind stress (Ketefian and Jacobson 2007). Water (ocean and lake) temperatures were also affected by sensible, latent, and radiative fluxes. Nine additional layers existed below each ocean mixed-layer grid cell to treat energy diffusion from the mixed layer to the deep ocean and ocean chemistry. Dissolution of gases to the ocean and ocean chemistry were calculated with OPD-EQUISOLV O (Jacobson 2005c), where OPD solves nonequilibrium transport between the ocean and atmosphere and EQUISOLV O solves chemical equilibrium in the ocean. Both schemes were mass conserving and unconditionally stable.

2.7. Agricultural Land and Other Surfaces

The model treated ground temperatures and moisture over subgrid surfaces (12 soil classes and roads, roofs, and water in each grid cell). It also treated vegetation over soil, snow over bare soil, snow over vegetation over soil, sea-ice over water, and snow over sea-ice over water (Jacobson 2001a). The initial soil moisture fields in all model domains were obtained from the monthly climatology of Nijssen et al. (2001). The fractional vegetation cover, necessary for these calculations, was obtained from the 1 kilometer (km) resolution dataset of Zeng et al. (2000). For all surfaces except sea ice and water, surface and subsurface temperatures and liquid water content were found with a time-dependent 10-layer module.

For each of the 12 subgrid soil classes in each grid cell, it was necessary to find the fractional agricultural land for applying irrigation. This fraction was determined from land use data at 1-km resolution (USGS 1999). The land use dataset consists of 24 landuse categories, one of which is assigned to each square kilometer. Five categories of data included agricultural land: dryland cropland and pasture, irrigated cropland and pasture, mixed dryland/irrigated cropland and pasture, cropland/grassland mosaic, and cropland/woodland mosaic. At each location in the model domain, the soil type (Miller and White 1998) and the landuse type were known at 1 km resolution. As such, it was possible to determine the fractional agricultural land

for each soil type in each model grid cell. Figure 1a shows the fractional agricultural land in each grid cell as a whole, which is the sum of the product of the agricultural fraction of each soil type and the fraction of the grid cell consisting of each soil type. The figure shows a strong agricultural presence in the San Joaquin Valley. Agriculture, though, existed throughout the model domain at lower levels. The figure also indicates that about 4.15% of all land area in the California model domain (which includes land area outside of California as well) consisted of an agricultural landuse category.

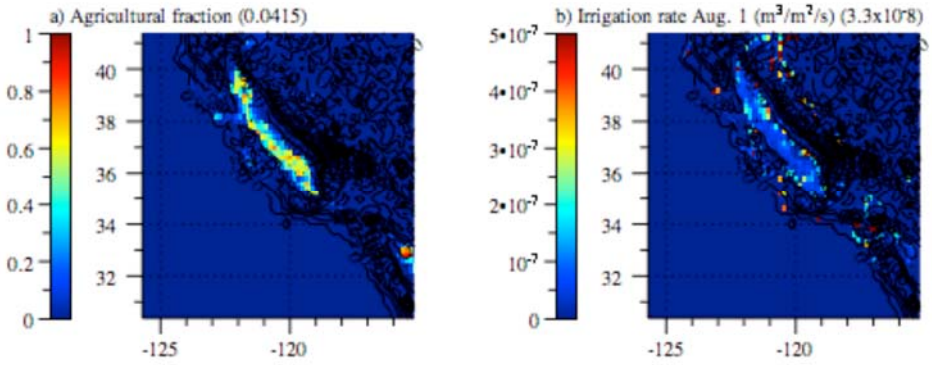

Figure 1. (a) Fraction of land as agriculture (USGS 1999), and (b) August 1 irrigation rate (Salas et al. 2006) in the model domain. The number in parentheses in each figure is the average value over all land points in the figure.

2.8. Irrigation

Irrigation data for the study were obtained from Salas et al. (2005). Data were available at 5-km resolution and daily temporal resolution for 1983, 1996, and 1997. Separate datasets were available for each year assuming either 1950s or early 2000s climate conditions. Here, the 1997 dataset with early 2000s climate conditions was used. The 5-km resolution data were converted to coarser model-resolution data in a water-conserving manner for each day of the year. Figure 1b shows an example of the resulting irrigation rates for August 1. The figure shows that most irrigation in California occurs in the San Joaquin Valley. Some irrigation occurs in the Eastern Los Angeles basin (approximately 118°W, 34°N) and to the east and northeast of San Diego (33°N).

Daily irrigation, which was now a model grid cell-average value, was applied proportionally to the fraction of agricultural land in each subgrid soil class in the grid cell. Thus, for example, if a grid cell consisted 50% of sandy loam and 50% clay loam, and the agriculture fraction of sandy loam was 30% and that of clay loam was 60%, one third of all irrigation in the cell was applied to the sandy loam soil class and two-thirds was applied to the clay loam class.

2.9. Treatment of Agricultural Albedo

Recent surface albedo data were obtained from a 1-km resolution dataset derived from Advanced Very High Resolution Radiometer (AVHRR) measurements for August 1990 (Martien and Umeda 1993). From these data, it was possible to calculate the albedo of land without agriculture mathematically as

$$A_{non-ag} = \frac{A_{cur} - A_{ag} f_{ag}}{1 - f_{ag}} \qquad (1)$$

where A_{cur} is the albedo of land from the data, A_{ag} is an assumed albedo of agricultural crops, and f_{ag} is the fraction of land occupied by agriculture (Section 2.7). The albedo of agricultural crops varies with season and type of crop. Gutman et al. (1989), for example, found that the visible albedo of corn in Iowa ranged from 0.12–0.14 in spring to 0.2–0.22 in August to 0.18 in September to 0.12 in October. Giambelluca et al. (1997) found the albedo of cropland in Brazil to range from 0.17-0.176. Here, albedo of agricultural land was estimated at A_{ag} =0.18. In addition, it was assumed that the albedo of land displaced by agriculture was that of nonagricultural land, as determined from Equation 1. Figure 2 shows both the baseline albedo (with agriculture) and the albedo difference (with minus without agriculture), derived from the baseline albedo data and Equation 1, respectively. The figure shows that agriculture may have increased the albedo of the northern and middle San Joaquin Valley but decreased the albedo of the southern valley. This result is consistent with the fact that the northern and middle valley was mostly rangeland and marshland (low albedo) and the southern 15% of the valley below Lake Tulare was (and still is) mostly desert, which has a high albedo, in the 1800s (Kahrl 1979). Thus, the addition of agriculture should increase the albedo of the northern and middle valley and decrease that of the southern valley, as found here.

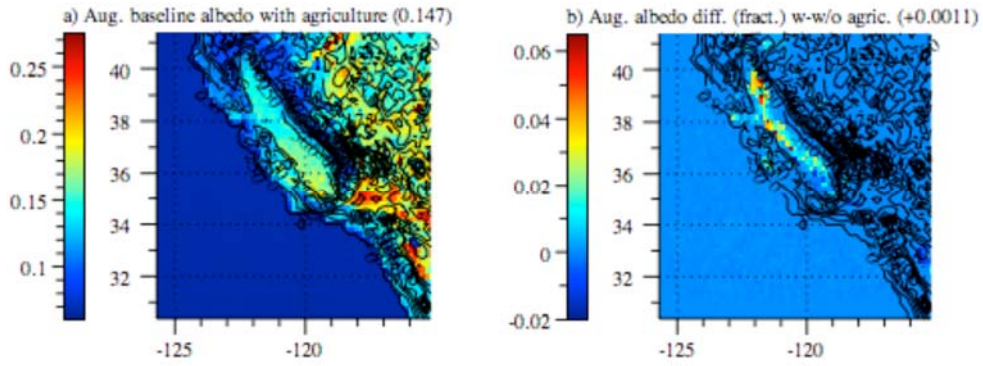

Figure 2. August baseline albedo (with agriculture) and the albedo difference between two simulations, one with and the other without agriculture. The number in parentheses in each figure is the average value over all land points in the figure.

2.10. Treatment of Black Carbon in Snow

Black carbon in the model entered snow by precipitation and dry deposition. Black carbon's concentration in snow was also affected by changes in snow depth due to melting, vapor deposition, and sublimation. Precipitation to the surface included size-resolved liquid, ice, and graupel. Aerosol components were carried to the surface in each size bin of each hydrometeor type. The calculation of dry deposition of soot to snow accounted for aerodynamic resistance, resistance to molecular diffusion, and the fall speed of particles. At the surface, snow and graupel were aggregated into one effective size bin for radiative calculations (r_{sn}=150 μm), which is in the range of typical effective radii used for snow optical calculations (e.g., Grenfell et al. 1994; Aoki et al. 2000). This radius was chosen for use here based on a best-fit of modeled to measured spectral albedo (Jacobson 2004). The effective radius of snow grains was assumed not to change due to snow aging, although in reality, snow aging causes the effective radius to increase and the albedo of new snow to decrease over time (e.g., Flanner et al. 2006). Because snow aging affects snow albedo when soot is both present and absent, not including it should have a somewhat minor effect on the albedo change due to soot in snow. For example, a 10% reduction in snow albedo due to aging combined with a 1% reduction in albedo due to soot causes a 0.1% error in the albedo change due to soot caused by not accounting for aging.

To account for radiative effects of BC in snow, one snow layer was added to the bottom of each atmospheric model column (which otherwise extended from the surface to 55 km) during radiative calculations. The wavelength-dependent upward irradiance divided by downward irradiance at the top of this layer was the calculated surface solar albedo (0.165 to 10 μm). The wavelength-dependent emissivity, used for spectral thermal-IR calculations (3 to 1000 μm), was one minus the calculated albedo. As such, the model predicted (rather than prescribed) the changes in albedo and emissivity of snow each radiative time step, and these change were affected by aerosol inclusions within snow and atmospheric optical properties. Because changes in albedo and emissivity affected incident solar radiation and heating, such changes affected the melting of snow, which fed back to soil moisture, albedo, and other climate variables.

Snow depth (D_s, cm) in the model was affected by precipitation and melting (Jacobson 2001a, Equation 36) as well as sublimation/ice deposition (added subsequently). Within each snow layer, it was necessary to calculate the concentration of BC. The time-dependent BC in snow (moles-BC cm^{-3}-snow) was calculated primarily as the sum of the concentrations of BC from precipitation and dry deposition, as described in Jacobson (2004). For snow-BC optical calculations, BC was treated as partly internally mixed as a core within snow grains and partly externally mixed from snow grains (in both cases, the BC was still internally mixed with other aerosol constituents). The refractive index of BC was taken from Krekov (1993). The density of emitted soot aggregates varies as a function of diameter and composition from 0.2–2.25 grams per cubic centimeter (g/cm^3) (e.g., Fuller et al. 1999). The value 1.5 g/cm^3 was chosen because it is relatively consistent with the mean size of emitted soot from Maricq et al. (2000, Figure 5), although no single number captures the density of soot.

Figure 3 shows the effect on spectral albedo of different levels of BC in snow. The result suggests that 25 nanograms per gram (ng/g) of BC might reduce the albedo of snow at 550

nanometers (nm) by 2.3%. Clarke and Noone (1985) similarly found that the addition of 25 ng/g of soot to snow decreased snow albedo by about 2.0%. The modeled effect of BC on emissivity is small. For example, at wavelength 7.75 μm, an increase from 0 to 500 ng/g BC increases emissivity by only 0.0005%.

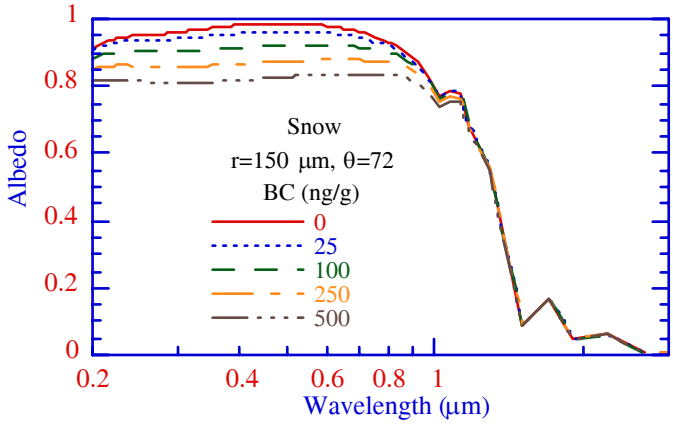

Figure 3. Comparison of modeled spectral albedos over snow containing different BC mass mixing ratios when each snow grain contains a single internally mixed BC inclusion and the rest of the BC in snow is assumed to be externally mixed (all BC particles in snow are assumed to be 266-nm diameter). The zenith angle (θ) was 72°. From Jacobson (2004).

3.0 Simulation Descriptions

Nested simulations were run to examine the effects of agriculture and absorption within snow on California climate and air pollution. Baseline and sensitivity simulations were conducted for both studies. For the agricultural study, simulations were run for August 2006; for the snow study, simulations were run for February 1999.

The model was run in nested mode from the global to regional scale. Two one-way nested domains were used: a global domain (4°-SN x 5°-WE resolution) and a California domain (0.2° x 0.15° ≈ 21.5 km x 14.0 km with the southwest corner grid cell centered at 30.0°N and -126.0°W and 60 SN cells x 75 WE cells). The global domain included 39 sigma-pressure layers between the surface and 0.425 hectopascal (hPa). The nested regional grids included 26 layers between the surface and 103.5 hPa, matching the bottom 26 global-model layers exactly. Each domain included five layers in the bottom 1 km. The nesting time interval for passing meteorological and chemical variables was one hour.

The gas and particle emission inventory used was the U.S. National Emission Inventory for 2002 (USEPA 2006a). The inventory accounted for over 370,000 stack and fugitive sources, 250,000 area sources, and 1700 source classification code (SCC) categories of on-road and non-road mobile sources. Pollutants emitted hourly included CO, CH_4, paraffins, olefins, formaldehyde, higher aldehydes, toluene, xylene, isoprene, monoterpenes, nitric oxide (NO), nitrogen dioxide (NO_2), nitrous acid (HONO), NH_3, sulfur dioxide (SO_2), sulfur trioxide (SO_3), sulfuric acid (H_2SO_4), particle black carbon, particle organic carbon, particle sulfate, particle nitrate, and other particulate matter. From the raw U.S. inventory, special inventories were prepared for each model domain. Particle mass emissions were spread over multimodal lognormal distributions. Additional emission types treated in the model were biogenic gases (isoprene, monoterpenes, and other volatile organics from vegetation and NO from soils), soildust, sea spray, pollen, spores, and bacteria, NO from lightning, dimethyl sulfide (DMS) from the oceans, volcanic SO_2, many gases and particles from biomass burning, and CO_2, hydrogen (H_2), and H_2O from fossil-fuel combustion and biomass burning.

For August 2006, a baseline simulation (with irrigation and current albedo) and two sensitivity simulations (one without irrigation but with current albedo and the other without irrigation and with pre-agriculture albedo) were run. For February 1999, a baseline simulation (with absorption by BC and soildust in snow) and one sensitivity simulation (without absorption in snow) were run. In the February baseline simulation, BC and soildust emissions, evolution, and absorption within snow were treated. In the sensitivity simulation, BC and soildust absorption within snow were not treated.

Sources of BC emissions in the model included shipping, aircraft, other fossil fuels, biofuels, and biomass burning. Land-based fossil-fuel soot (BC, OM, and sulfate) emissions were obtained from USEPA (2006a) within the United States and Bond et al. (2004) outside the United States. Shipping BC emissions were obtained by scaling BC emission factors to the sulfur shipping emission rate from Corbett et al. (2003), as described in Jacobson (2006). Aircraft BC emissions inventory were derived by applying BC emission factors to the 1999 commercial, military, and

charter aircraft fuel use data of Sutkus et al. (2001) and Mortlock and Van Alstyne (1998). Soildust emissions as a function of size, soil type, wind speed, soil moisture, and snow cover were calculated with the method of Marticorena et al. (1997) using soil data from Miller and White (1998).

The global domain simulations were the same for both baseline and sensitivity California-domain simulations to ensure that errors due to coarser resolution in the global domain did not influence results in the finer California domain.

The model dynamics time steps were 300 seconds (s) (global domain) and 10 s (California domain). The time interval for nesting between the domains was one hour. Nesting was treated using a five-row buffer layer at each horizontal boundary in each fine domain to relax concentrations and other variables from the coarse domain, as in Jacobson (2005d, Section 21.1.11). Variables passed at the horizontal boundaries included temperature, specific humidity, wind velocity, gas concentrations (including total water as water vapor), and size- and composition-resolved aerosol concentrations. Clouds themselves were treated with no-flux boundary conditions, since total water as water vapor moved across boundaries and could generate new clouds; however, there is no reason why clouds could not be passed across the boundaries as well for future studies.

For February 1999, initial meteorological fields were obtained from National Center for Environmental Prediction (NCEP) reanalysis fields for February 1, 1999, at 12 Greenwich Mean Time (GMT) (NCEP 2003). Aerosol and gas fields in all domains were similarly initialized from background data. U.S. Environmental Protection Agency (EPA) ambient air quality data (USEPA 2006b) for O_3, CO, NO_2, SO_2, particulate matter ≤ 2.5 micrometers in diameter ($PM_{2.5}$), and particulate matter ≤ 10 micrometers in diameter (PM_{10}) were then assimilated with background values at the initial time. For August 2006, initial meteorological fields were obtained from Global Forecast System (GFS) 1^o x 1^o data. No data assimilation, nudging, or model spinup was performed during any simulation and gas/aerosol fields were initialized from background values.

4.0 Effects of Agriculture

Figure 4 shows baseline and sensitivity simulation results related to agriculture. Each subfigure includes (in the upper right corner), the average parameter value over all land in the figure, which includes land in California and parts of Nevada. Table 2 summarizes statistics from the figures and figures not shown. Statistics over land rather than irrigated land only are shown, because the latter does not capture feedbacks to areas beyond those irrigated, particularly populated cities. Although irrigation data were available for California only, Figure 1a shows that Nevada has little agricultural land relative to California, so the lack of irrigation data for Nevada should not result in significant error in the estimated effects of irrigation on all land-averaged atmospheric properties.

The irrigation of agriculture (without considering albedo change) resulted in an increase in soil moisture, averaged over all land in the California model domain during August, of about 6% (Table 2, Figure 4a). Most of the increases occurred in the San Joaquin Valley, where monthly averaged soil moisture increased by up to 0.15 m^3/m^3. When both irrigation and albedo change due to agriculture were accounted for, soil moisture similarly increased in the San Joaquin Valley (Figure 4a).

Irrigation of agriculture also occurs in the Imperial Valley, located near 115°W, 33°N, as seen in Figure 1a. However, because this area was predominantly in the five-row buffer area of the California model domain where parameters were relaxed to global-domain values during nesting, feedbacks of agriculture to atmospheric properties in the Imperial Valley were dampened and should not be relied on here. Some portions of the eastern Los Angeles basin (118°W, 34°N) were also irrigated, but to a lesser extent than in the San Joaquin Valley, so soil moisture changes there were smaller than in the valley.

The increase in soil moisture due to irrigation increased evaporation, which increased monthly averaged water vapor over land by about 0.25% (Table 2, Figure 4b), the relative humidity by near 0.5% (Table 2, Figure 4c), cloud optical depth by near 8% (Table 2, Figure 4d), and cloud fraction by about 5% (Table 2, Figure 4e). Peak monthly averaged local relative humidity increases in the San Joaquin Valley were about 8% (Figure 4c).

The measured climatological precipitation in the San Joaquin Valley in August is low but not zero. It is higher in the northern valley and lower in the southern valley. Some measured August climatological precipitation rates in the valley are 0.15 mm/day in Orland and Hamilton City, 0.09 mm/day in St. John, 0.08 mm/day in Oroville, 0.066 mm/day in Knights Landing, 0.06 mm/day in Williams and Colusa, 0.016 mm/day in Madera, and 0.008 mm/day in Tulefield and Benson's Ferry (Western Regional Climate Center 2006). Measured precipitation is really the difference between precipitation and evaporation in the rain gauge. Modeled precipitation rates were absolute precipitation values, because evaporation was calculated separately. This partly explains why modeled baseline August precipitation in the valley (Figure 4f) was generally higher in the San Joaquin Valley than was climatological precipitation. The modeled precipitation was primarily from nighttime and early-morning fog deposits/drizzle rather than from convective clouds. Much of the modeled precipitated water re-evaporated during the day.

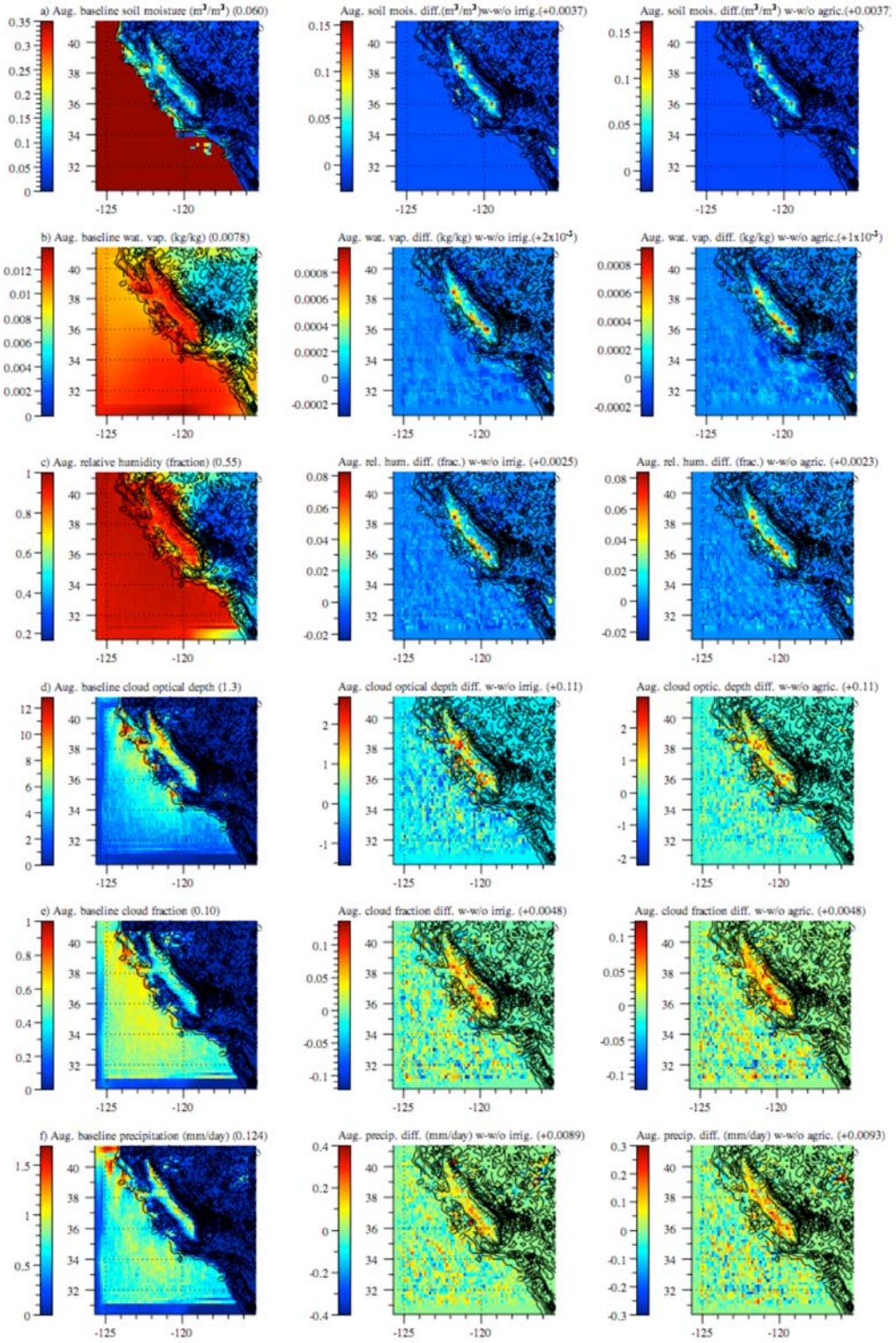

Figure 4. Modeled August-averaged baseline values (with irrigation and current albedo of agriculture) (left panel), baseline values minus those without irrigation (w-w/o irrig.) (middle panel), and baseline values minus those without irrigation and with pre-agriculture albedo (w-w/o agric.) (right panel) for several parameters in the California domain. Each number in parentheses is the average value over all land points.

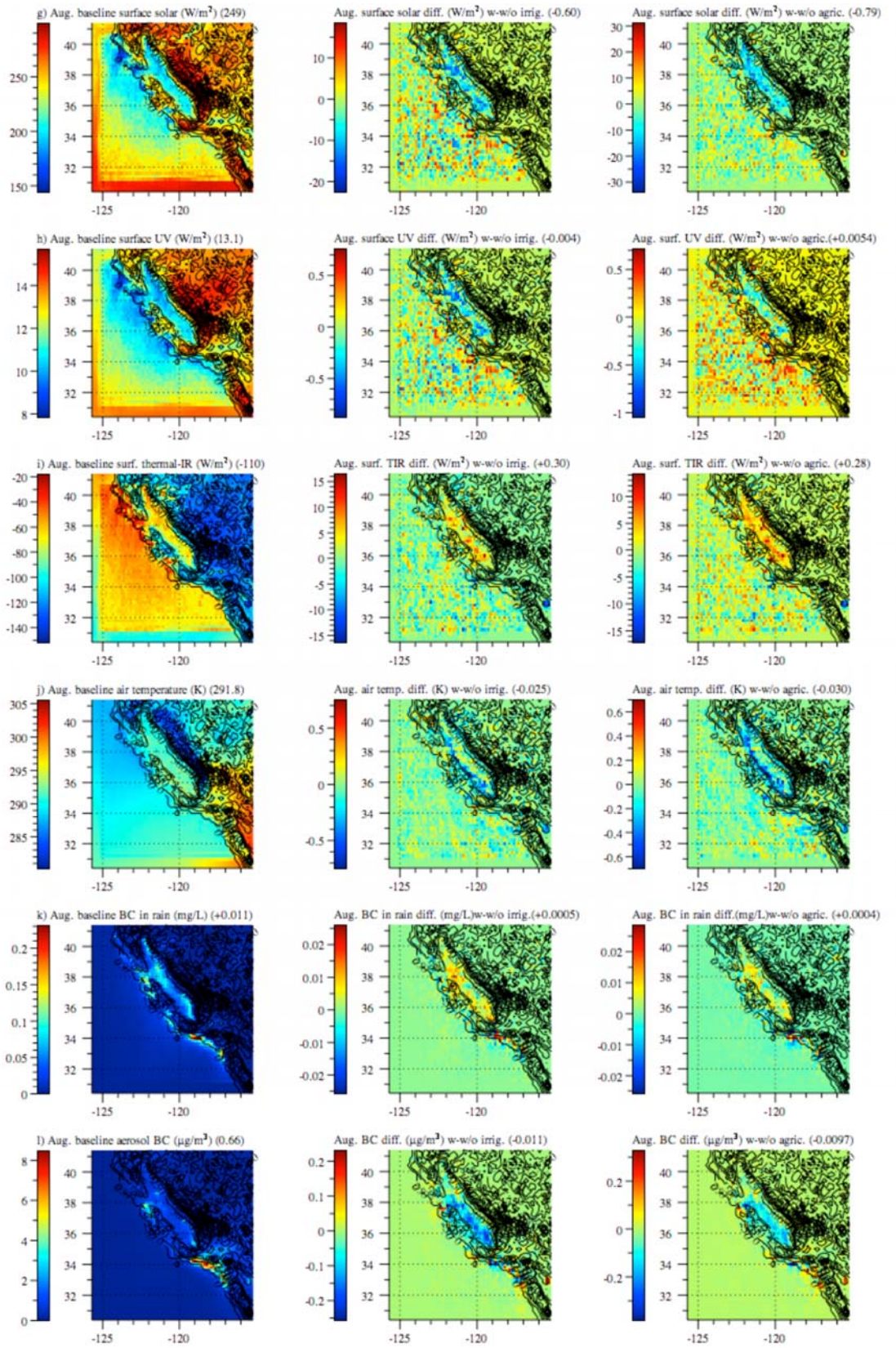

Figure 4. continued.

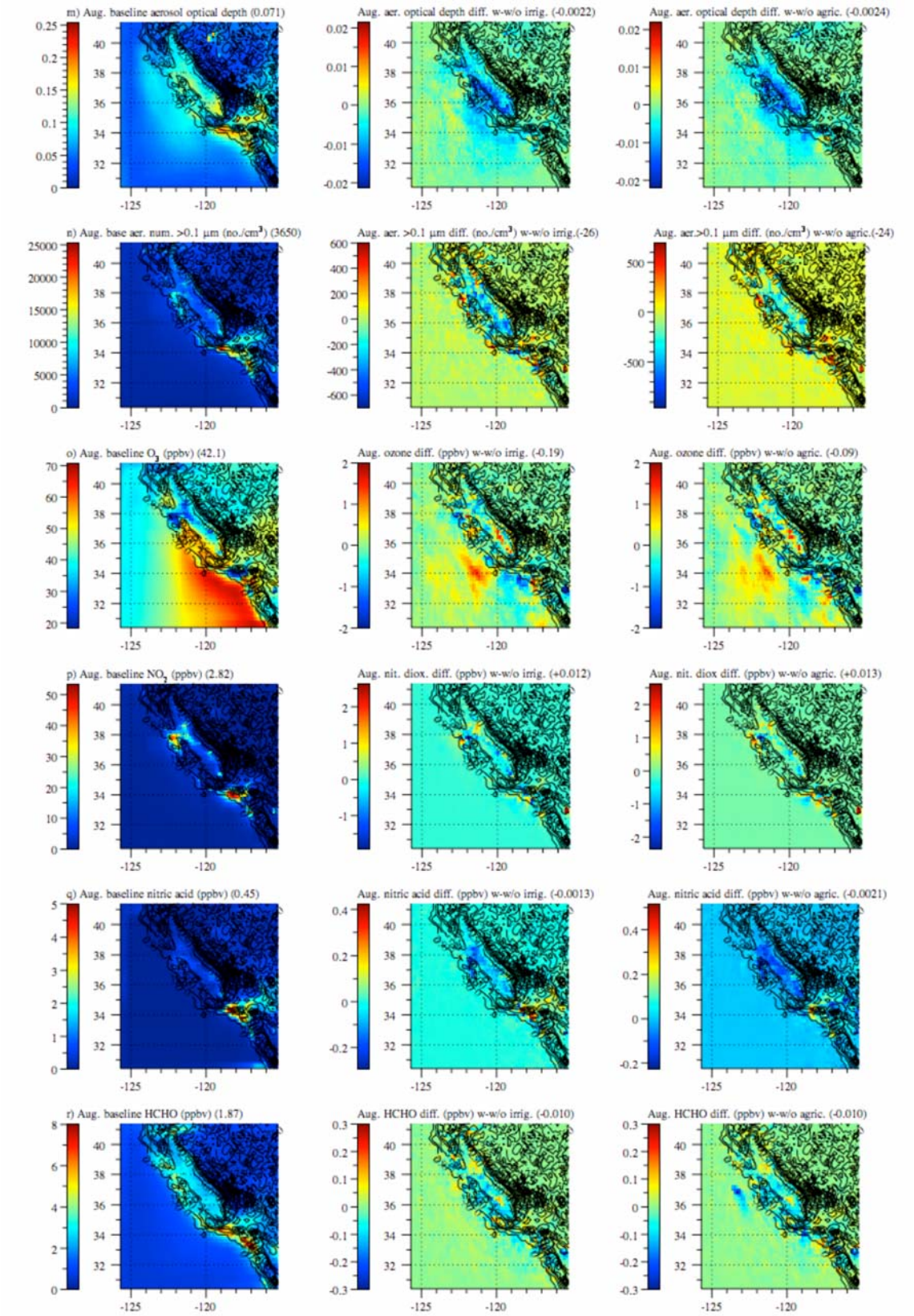

Figure 4. continued.

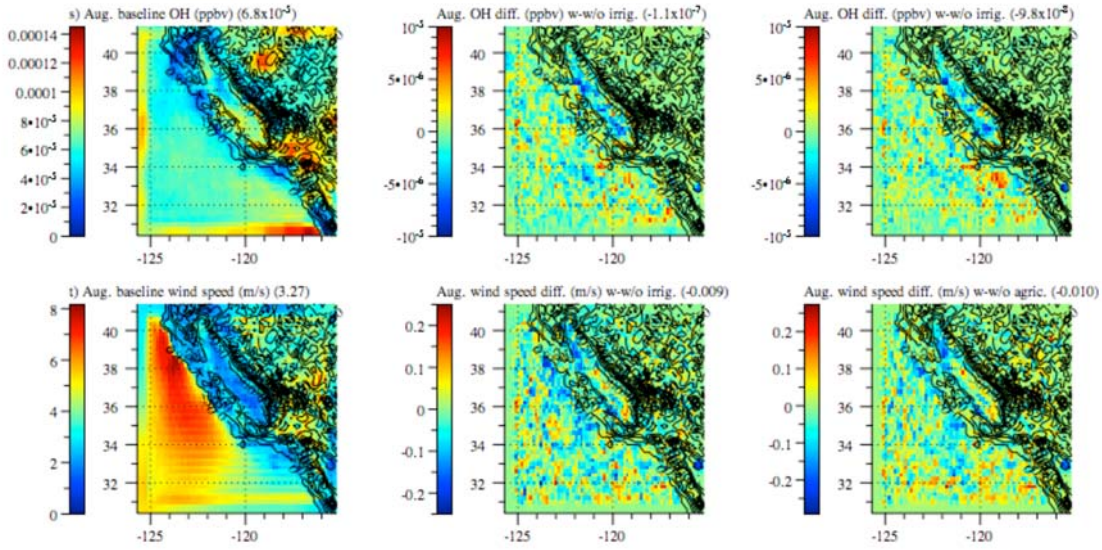

Figure 4. continued.

Increases in soil moisture due to irrigation increased modeled precipitation by 7.2%, with most changes occurring in the San Joaquin Valley (Table 2, Figure 4f). With generally low precipitation levels in August, a 7.2% increase in precipitation is not a significant quantity of water. In the irrigation plus albedo case, precipitation increased by 7.5%.

The greater cloud optical depth due to irrigation reduced surface solar irradiance (Figure 4g) and UV irradiance in the San Joaquin Valley (Figure 4h) but increased thermal-IR irradiance there (Figure 4i). The net effect of the radiation changes together with the soil moisture changes due to irrigation was to decrease near-surface air temperatures by a land average of 0.025 K, with peak reductions of about 0.7 K in parts of the San Joaquin Valley (Figure 4j). The inclusion of albedo changes due to agriculture reduced temperatures further, by a total land-average of 0.03 K (Figure 4j). Thus, the net increase in albedo of up to 6% locally in California due to agriculture (Figure 2b) had a measurable impact on land-averaged temperature.

The effect of irrigation on air temperatures was net cooling; however, irrigation generally warmed the air slightly at night but cooled it to a greater extent during the day (Figure 5), reducing the magnitudes of both temperature maximums and minimums.

Table 2. Modeled August-averaged baseline values (with current irrigation and albedo due to agriculture) over all irrigated and nonirrigated land points and percent changes in mean values due to irrigation alone ("irrigation") and irrigation plus albedo change ("agriculture"). Results correspond to several of the panels in Figures 3 and 4.

	Baseline	Percent change w minus w/o irrigation	Percent change w minus w/o agriculture
Albedo (fraction)	0.147	0	+0.76
Soil moisture (m^3/m^3)	0.060	+6.2	+6.2
Water vapor (kg/kg)	0.0078	+0.25	+0.16
Relative humidity (fract.)	0.553	+0.45	+0.42
Cloud optical depth	1.3	+8.3	+8.1
Cloud fraction	0.10	+4.6	+4.6
Precipitation (mm/day)	0.124	+7.2	+7.5
Surface solar (W/m^2)	249	-0.24	-0.32
Surface UV (W/m^2)	13.1	-0.033	+0.004
Surface thermal-IR (W/m^2)	-110	+0.27	+0.26
Air temperature (K)	291.8	-0.0085	-0.010
Wind speed (m/s)	3.3	-0.28	-0.30
BC in rain (mg/L)	0.011	+4.4	+3.6
Aerosol BC ($\mu g/m^3$)	0.66	-1.6	-1.5
Cloud BC ($\mu g/m^3$)	0.027	+3.3	+2.3
Aerosol POM ($\mu g/m^3$)	6.25	-1.3	-1.2
Cloud POM ($\mu g/m^3$)	0.25	+2.8	+1.8
Aerosol SOM ($\mu g/m^3$)	3.20	-2.7	-2.7
Cloud SOM ($\mu g/m^3$)	0.096	+2.8	+2.2
Aerosol LWC ($\mu g/m^3$)	4.50	-7.2	-7.1
Cloud LWC (kg/m^2)	0.0053	+8.1	+7.8
Aerosol S(VI) ($\mu g/m^3$)	0.44	-1.3	-1.2
Cloud S(VI) ($\mu g/m^3$)	0.045	+2.5	+2.6
Aerosol NH_4^+ ($\mu g/m^3$)	0.27	-8.6	-8.0
Cloud NH_4^+ ($\mu g/m^3$)	0.015	-2.4	-2.7
Aerosol NO_3^- ($\mu g/m^3$)	0.70	-10.5	-9.5
Cloud NO_3^- ($\mu g/m^3$)	0.028	-6.5	-7.1
Aerosol extinction (m^2/g)	2.23	-0.17	-0.35
Aerosol optical depth	0.071	-3.2	-3.3
Aerosol > 0.1 μm (No/cm^3)	3650	-0.71	-0.65
Nitric oxide (ppbv)	0.65	+0.96	+1.2
Nitrogen dioxide (ppbv)	2.82	+0.43	+0.46
Carbon monoxide (ppbv)	174	+0.19	+0.23
Methane (ppbv)	1720	+0.016	+0.014
1,3-butadiene (ppbv)	0.020	+0.36	+0.26
Benzene (ppbv)	0.086	+0.40	+0.5
PAN (ppbv)	0.40	+0.3	+0.36
Nitric acid (ppbv)	0.45	-0.28	-0.48
Formaldehyde (ppbv)	1.87	-0.55	-0.55
Sulfur dioxide (ppbv)	0.30	-1.6	-1.5
Hydroxyl radical (ppbv)	0.000068	-0.16	-0.14
24-hour ozone (ppbv)	42.1	-0.19	-0.21
Daytime ozone (ppbv)	49.1	-0.25	-0.27

m^3/m^3=cubic meter by cubic meter; kg/kg=kilogram per kilogram; mm/day=millimeters per day; W/m^2=watts per square meter; K=kelvin; m/s=meters per second; mg/L= milligrams per liter; $\mu g/m^3$=micrograms per cubic meter; kg/m^2=kilogram per square meter; m^2/g=square meter per gram; S(VI)=aerosol sulfate; No/cm^3=number per cubic centimeter; ppbv=parts per billion volume; PAN=peroxyacetyl nitrate

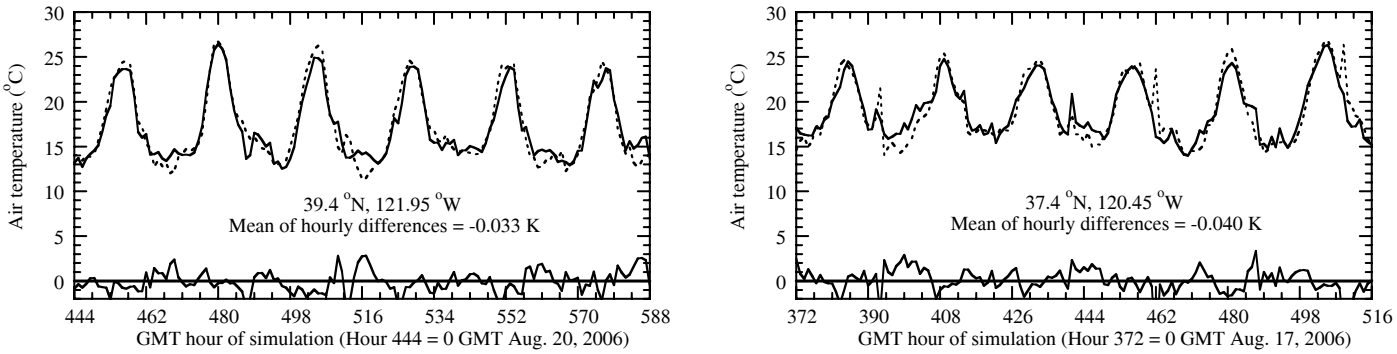

Figure 5. Time-dependent variation for several days in August in modeled near-surface air temperature at two locations when irrigation was included (solid lines) and excluded (dashed lines). The "Mean of hourly differences" is the mean over all hours of the month of August, only some of which are shown in the figure.

The net cooling of near-surface air and increase in precipitation due to agriculture (irrigation plus albedo change) found here is consistent in direction with the data analysis results of Barnston and Schickedanz (1984) but also with Moore and Rojstaczer (2001), who concluded that the magnitude of precipitation change due to agriculture may be small. The cooling due to agriculture is also consistent with results from Adegoke et al. (2003), Boucher et al. (2004), Snyder et al. (2006), and Lobell et al. (2006). Because agriculture appears to have increased rather than decreased the albedo over most of the San Joaquin Valley, the net warming found in the valley by Christy et al. (2006) may be due to other factors (e.g., anthropogenic greenhouse gas and absorbing particle warming) rather than an increase in agriculture as speculated therein. The observed warming in the valley is unlikely to be due to the sum of all anthropogenic aerosol particles; Jacobson and Kaufman (2006), for example, found a net cooling (nighttime warming and greater daytime cooling) due to such particles in the San Joaquin Valley. Although black carbon in aerosol particles causes warming, it is dominated by larger amounts of scattering aerosol particles.

The increase in drizzle in the San Joaquin Valley due to irrigation increased the concentration of pollutants in rainwater, increasing wet removal of these pollutants. For example, irrigation alone increased the concentration of BC in cloud water by about 3.3% (Table 2) and rainwater by about 4.4% (Table 2, Figure 4k) and decreased it in air by about 1.6% (Table 2, Figure 4l) on average over all land, but mostly in the San Joaquin Valley. Due to enhanced drizzle, irrigation similarly decreased aerosol POM, SOM, S(VI), ammonium (NH_4^+), and nitrate (NO_3^-) (Table 2). Although a higher relative humidity (Table 2) tended to increase aerosol liquid water content (ALWC), the removal of hydrating aerosol constituents caused a net decrease in ALWC (Table 2). The net effect of irrigation, therefore, in the San Joaquin Valley was to decrease aerosol extinction (Table 2), optical depth (Table 2, Figure 4m), and number (Table 2, Figure 4n).

Irrigation slightly increased the near-surface mixing ratios of low-solubility, slowly reacting gases, such as CO, CH_4 (Table 2) by reducing the mixing depth and decreasing the near-surface wind speed (Table 2). It reduced the mixing depth by cooling the ground (Table 2, Figure 4j),

thereby increasing stability. The enhanced stability reduced turbulent kinetic energy and shearing stress, which reduced vertical transport of faster winds aloft to the surface. Irrigation slightly increased the near-surface mixing ratios of low-solubility, slowly reacting gases, such as CO, CH_4 (Table 2) by (a) cooling the ground (Table 2, Figure 4j), thereby increasing stability and reducing the mixing depth, and (b) decreasing the near-surface wind speed (Table 2, Figure 4t). Irrigation reduced wind speed by cooling the surface, thereby increasing stability, reducing turbulent kinetic energy, shearing stress, and the vertical transport of faster winds aloft to the surface. Irrigation decreased the near-surface mixing ratios of soluble gases, such as HNO_3 (Figure 4q), formaldehyde (HCHO) (Figure 4r), and SO_2 (Table 2) by increasing cloud liquid water and precipitation. The reduction in aldehydes and UV radiation (Figure 4h) reduced OH in the valley (Figure 4s). The reduction in UV radiation and increase in near-surface NO and NO_2 (Table 2, Figure 4p) in the northern San Joaquin Valley helped to decrease near-surface ozone in the northern valley (Figure 4o) and increase PAN, on average over land (Table 2). A decrease in nitrogen oxides in the southern valley (Figure 4p) contributed to an ozone increase there (Figure 4o).

Table 2 indicates that percent changes in several parameters due to irrigation were relatively small. This might suggest that the magnitude and direction of the modeled changes could be random. However, if the changes were random, the results would change randomly upon a change in the initial conditions or of a parameterization in the model and would not follow what might be expected from physical principles. However, Table 2 indicates that, when a second sensitivity test was run for each domain (e.g., when both albedo and irrigation were perturbed) the percent changes were close to those when only irrigation was perturbed. Further changes in both sensitivities could be explained in terms of physical principles. As such, it appears unlikely that the sign of the changes found were random or noise but were real responses to irrigation and/or albedo changes. The magnitudes of the changes are more uncertain and would undoubtedly change further upon an improvement in model resolution and physical processes treated.

5.0 Effects of Impurities in Snow

February 1999 was a moderately wet year in Northern California but dry in the Southern part of the state (Figure 6). Most precipitation occurred along the northern coast and in the Sierra Nevada Mountains. The model was able to predict the locations of strong and weak precipitation, as well as the magnitude in many locations, although it overpredicted the magnitude in the Sierra by about a third (Figure 6). Part of this error may be due to coarse model resolution (21.5 km x 14.0 km) and to initialization with the coarsely resolved NCEP reanalysis (2.5° x 2.5°).

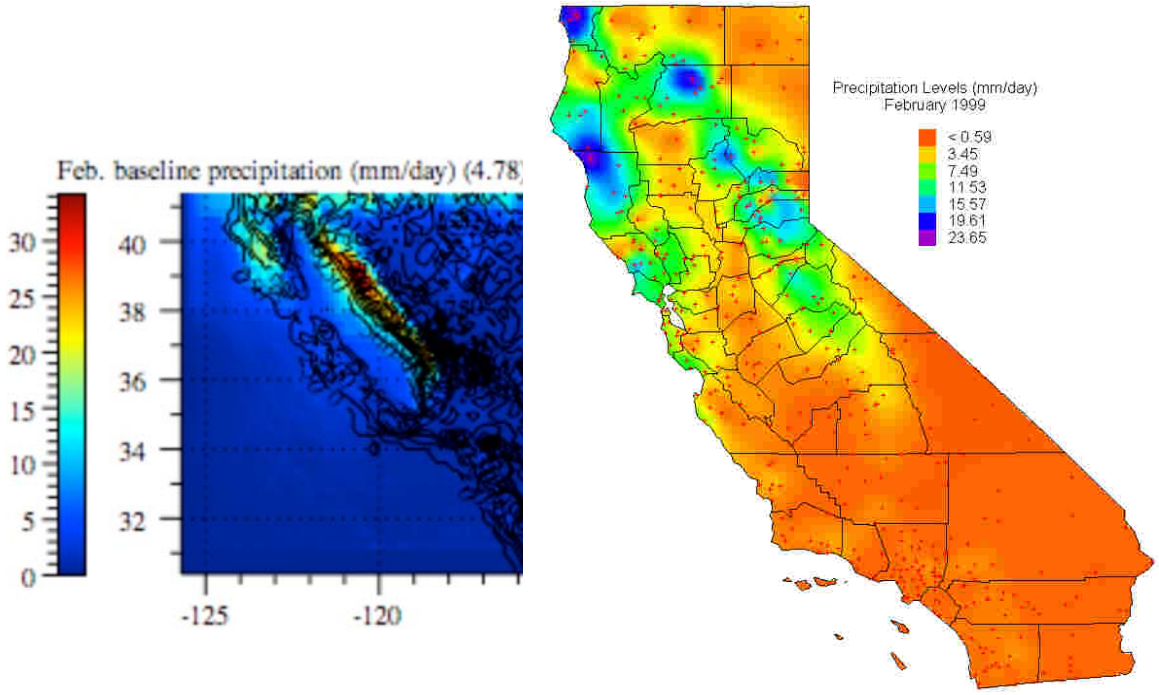

Figure 6. Modeled versus measured February precipitation

Most of the modeled snow fell in the Sierra, although a small amount fell in Northern and Eastern Nevada as well (Figure 7a), as indicated by the higher albedos there (Figure 7b). Black carbon and soildust in the model were tracked through aerosols, clouds, rain, and snow (Figures 7c, 7d). Both entered snow by wet and dry deposition. Whereas nearly all BC in the model was anthropogenic, most soildust was natural and produced by the wind passing over loose sand or dirt.

Table 3. Summary of February modeled mean baseline values over all land points in the model domain and percent changes in mean values due to BC and soildust absorption in snow. Data correspond to Figure 7.

	Mean baseline value (with absorption in snow)	Mean percent change with minus without absorption in snow
Snow depth (m)	0.0217	-0.41
Albedo (fraction)	0.247	-0.32
BC in air ($\mu g/m^3$)	0.287	-0.02
BC in cloud particles ($\mu g/m^3$)	0.027	+0.27
BC in rain (mg/L)	0.011	+0.20
BC in snow (mg/L)	0.0023	-1.8
Soildust in air ($\mu g/m^3$)	0.187	-3.1
Soildust in cloud part. ($\mu g/m^3$)	0.009	-3.6
Soildust in rain (mg/L)	0.082	+2.1
Soildust in snow (mg/L)	0.058	+4.3
Ground temperature (K)	276.75	+0.004
Soil moisture (m^3/m^3)	0.289	+0.07
Relative humidity (fraction)	0.83	+0.048
Cloud optical depth	5.45	-0.18

Absorption of solar radiation by BC and soildust together in snow reduced snow depth by about 0.4% (Table 3, Figure 7a) and surface albedo by about 0.32% (Table 3, Figure 7b) in February in the California domain over all land points (snow covered and non-snow-covered). Maximum snow depth and albedo decreases over snow were 2% and 4%, respectively. For comparison, Jacobson (2004) calculated that BC alone reduced snow and sea ice albedo by 0.4% in the annual and global average and 1% in the Northern Hemisphere. The larger effects on the global scale were attributable to the feedbacks that operated over a much longer time in that study. Also, the Arctic and Northern Europe/Asia, where most of the black carbon effects occurred on the global scale, have nearby sources of BC (e.g., Europe and Asia) greater in magnitude than does California (mostly the San Joaquin Valley, Los Angeles, and San Francisco).

The increased absorption by BC and soildust in snow increased the modeled ground temperature in February over all land by about 0.11 K (0.004%) (Table 3, Figure 7e). For comparison, the global and annual average increase in near-surface air temperatures due to BC absorption alone in snow was about 0.06 K (Jacobson 2004).

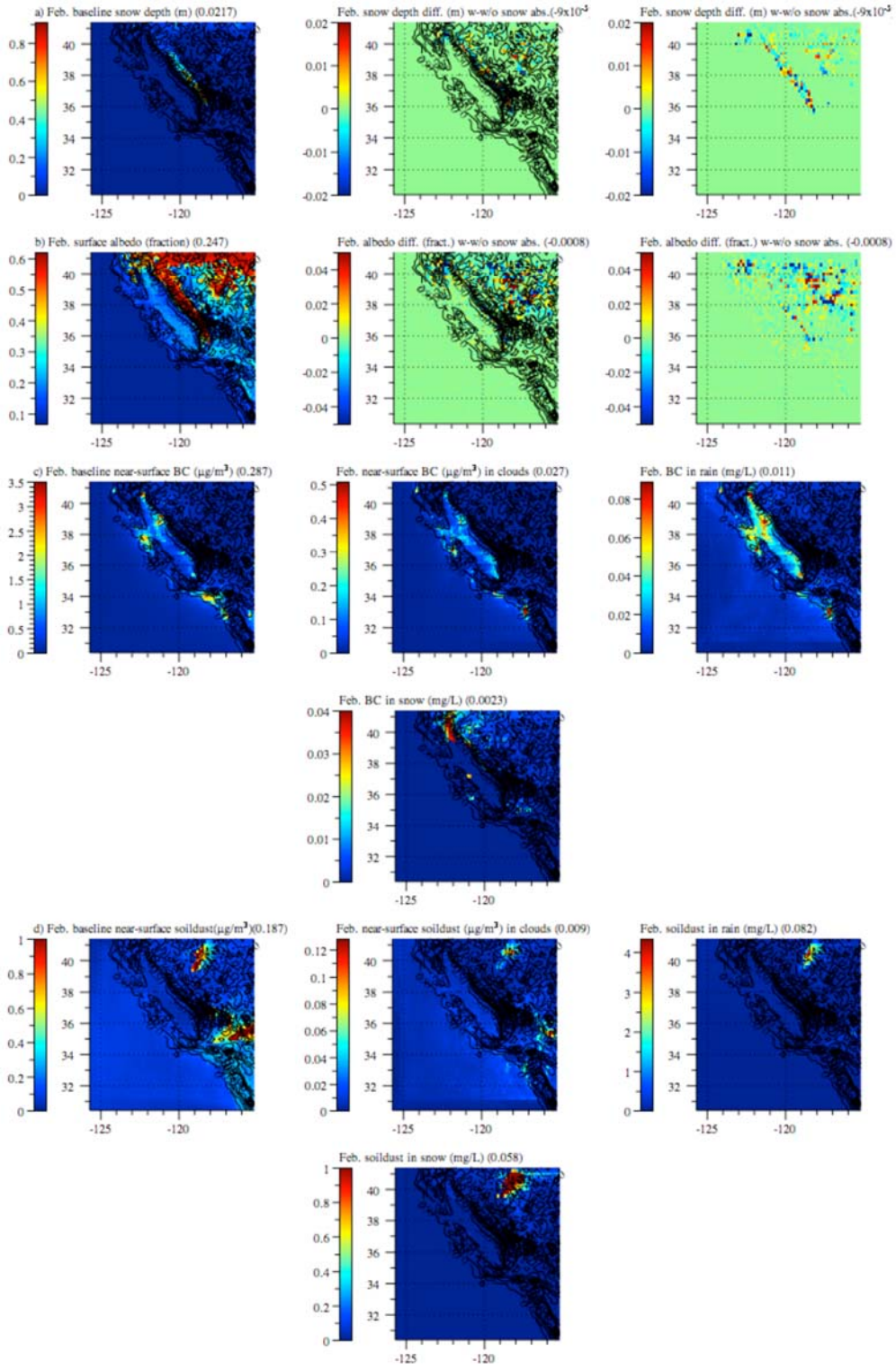

Figure 7. Modeled February-averaged baseline values (with absorption by BC and soildust in snow) and values with minus without such absorption (w-w/o snow abs.) for several parameters. The number in parentheses in each figure is the average value over all land points (snow-covered and non-snow covered) in the figure. In some cases, a difference figure without topography is shown. Such figures have the same data as the difference figure without topography.

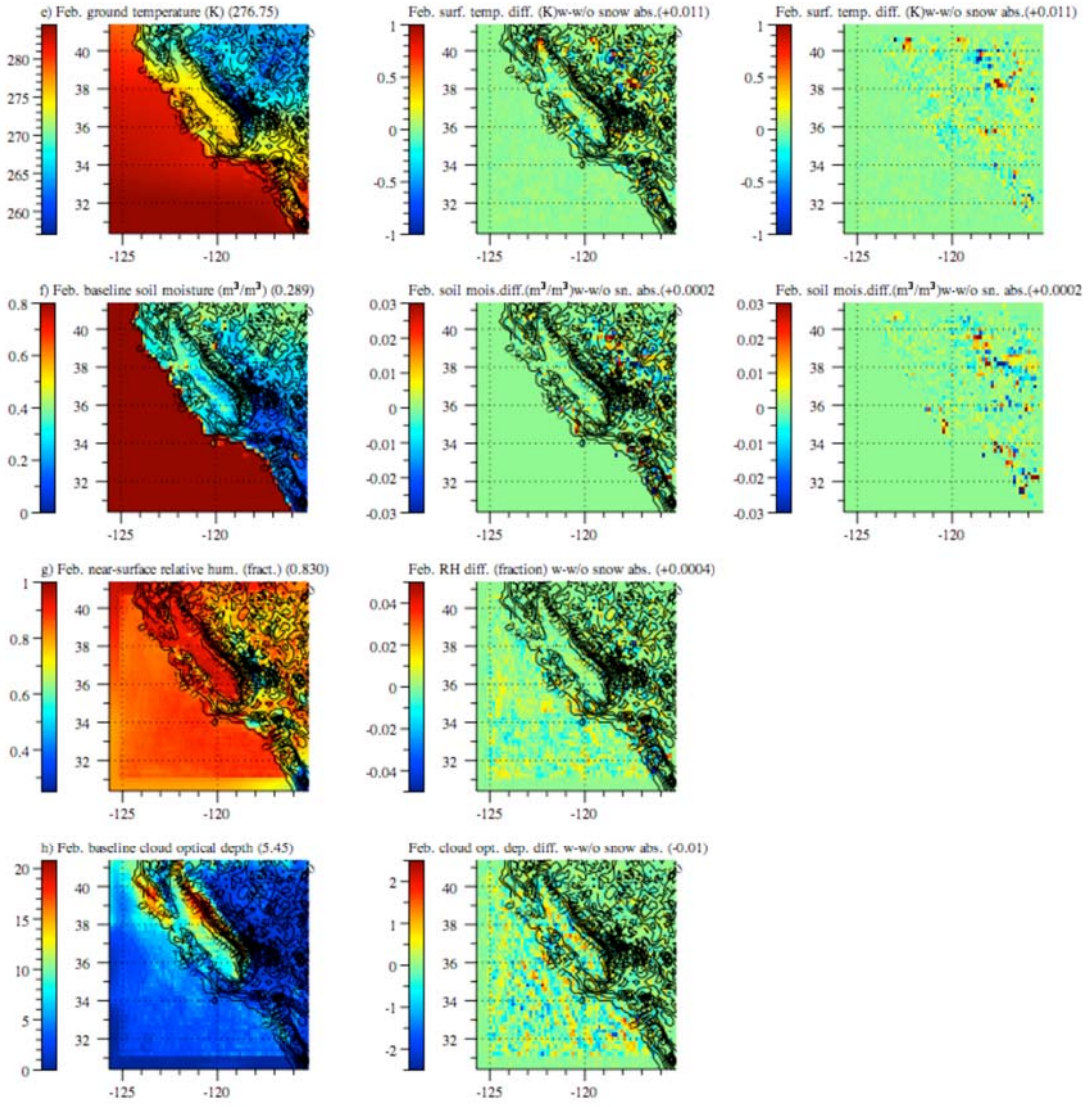

Figure 7. continued.

The reduction in snow due to absorption was compensated for in part by increases in meltwater and water vapor. Snow absorption increased soil moisture by about 0.07% (Table 3, Figure 7f), water vapor by about 0.1%, and the relative humidity by about 0.05% (Table 3, Figure 7g). The increase in soil moisture suggests a hastening of the release of meltwater due to absorption by impurities in snow. The increase in water vapor together with the loss in snow depth suggests a net reduction in water supply due to such impurities.

The rate of snowmelt depends on ambient temperatures and temperature changes due to impurities in snow. In April, ambient temperatures are higher, so more snow melts then than it does in February, as indicated by the snow depth statistics discussed in Section 1. Similarly, the same level of impurities in snow speeds melting of snow in April more than in February

because incident solar radiation, thus solar absorption and thermal-infrared heating by impurities, is greater in April. Finally, because less snowfall occurs in April than in February, more impurities can accumulate on top of snow without being buried by new snow in April. On the other hand since more snow is present in February, impurities in snow cause feedbacks over a larger region in February than in April. Overall, it is estimated that the results here for February may underestimate the effects of impurities on snowmelt relative to April.

Finally, the higher water vapor in the San Joaquin Valley resulted in a slight increase in cloud optical depth there (Figure 7h), although the land-averaged change in optical depth was negative (Table 3).

6.0 Conclusions

This report discussed the effects of irrigation and albedo change attributable to agriculture on California weather, climate, and air pollution; and the effects of black carbon and soildust absorption within snow on snowmelt and the subsequent feedback to California's climate. Numerical simulations were run for August 2006 to examine the first issue and for February 1999 to examine the second issue.

Satellite albedo data and irrigation data were obtained to examine the first issue. An inversion method was combined with the satellite data to estimate California's albedo in the absence of agriculture. It was found that agriculture may have increased the albedo of the northern and middle San Joaquin Valley but decreased the albedo of the southern valley relative to the albedo in the 1800s. Such a result implies that, when only albedo is considered, agriculture should cause a slight cooling of the valley. Irrigation should also cause cooling during the day but a warming at night.

The numerical simulations showed that irrigation alone decreased near-surface air temperatures by about 0.025 K and irrigation-plus-albedo changes decreased temperatures by about 0.03 K in the monthly average over land in the model domain (covering California and parts of Nevada). Nighttime temperatures increased while daytime temperatures decreased to a greater extent. Maximum local decreases in August temperatures were about 0.7 K, occurring in the San Joaquin Valley. Since agriculture caused a net summer cooling of the San Joaquin Valley, the valley's observed historic warming appears more likely due to anthropogenic greenhouse gas buildup than to agriculture. Irrigation increased soil moisture by an average over land of about 6%, the relative humidity by about 0.4%, cloud optical depth by about 8%, cloud fraction by about 5%, and drizzle by about 7%.

Increased stability from irrigation decreased wind speeds. Both factors increased the near-surface mixing ratios of low-solubility, slowly reacting gases, such as CO and CH_4. By increasing cloudiness and wet removal, agriculture decreased the mixing ratios of soluble gases, such as HNO_3 and SO_2. Thus, irrigation reduced primary pollutant concentrations when precipitation or drizzle was imminent or present but increased such pollution when precipitation was absent. Reductions in UV radiation and increases in nitrogen oxides due to irrigation slightly decreased ozone in California.

With respect to the effects of impurities in snow, absorption of solar radiation by black carbon and soildust in snow reduced land albedo in February by about 0.3%, reduced land-averaged snow depth by about 0.5%, increased ground temperatures over land by about 0.11 K, increased soil moisture by about 0.07%, and increased the relative humidity by about 0.04% over land. This result implies that impurities in snow may decrease water supply by increasing sublimation and may hasten the release of meltwater.

Although the effects of impurities on snow melting should be greater in April than in February, due to warmer temperatures and greater solar radiation in April, snow area in April is much lower than in February, so newly deposited impurities from Asia may have a lesser aggregate impact on snowmelt by the time they arrive in April, than local impurities, which are deposited

over a larger snow area and over a longer period prior to April. Nevertheless, this study implies that efforts to reduce both local and Asian particle emissions will help to alleviate slightly the effect of climate change on early release of meltwater. Reducing emissions have the additional benefit of improving human health.

Whereas the modeled signs of changes due to agriculture and impurities in snow may be relatively reliable, the magnitudes are less certain. Such uncertainty can be reduced by improving model resolution; initialization; treatment of physical, chemical, and dynamical processes; and input datasets.

7.0 References

Adegoke, J. O., R. A. S. Pielke, J. L. Eastman, R. Mahmood, and K.G. Hubbard. 2003. "Impact of irrigation on midsummer surface fluxes and temperature under dry synoptic conditions: A regional atmospheric model study of the U.S. High Plains." *Monthly Weather Review* 131: 556–564.

Aoki, T., T. Aoki, M. Fukabori, A. Hachikubo, Y. Tachibana, and F. Nishio. 2000. "Effects of snow physical parameters on spectral albedo and bi-directional reflectance of snow surface." *J. Geophys. Res*. 105: 10,219–10,236.

Arakawa, A., and V. R. Lamb. 1981. "A potential enstrophy and energy conserving scheme for the shallow water equations." *Mon. Wea. Rev*. 109: 18–36.

Barnston, A., and P. T. Schickedanz. 1984. The effect of irrigation on warm season precipitation in the southern Great Plains. *J. Climate Appl. Meteor.* 23: 865–888.

Bond, T. C., D. G. Streets, K. F. Yarber, S. M. Nelson, J.-H. Woo, and Z. Klimont. 2004. "A technology-based global inventory of black and organic carbon emissions from combustion." *J. Geophys. Res*. 109: D14203, doi: 10.1029/2003JD003697.

Boucher, O., G. Myhre, A. Myhre. 2004. "Direct human influence of irrigation on atmospheric water vapor and climate." *Climate Dynamics* 22: 597–603.

Christy, J. R., W. B. Norris, K. Redmond, and K. P. Gallo. 2005. Methodology and results of calculating Central California surface temperature trends: Evidence of human-induced climate change? *J. Clim.* 19: 548–563.

Chylek, P., V. Ramaswamy, and V. Srivastava. 1983. "Albedo of soot-contaminated snow." *J. Geophys. Res*. 88: 10,837–10,843.

Chylek, P., V. Srivastava, L. Cahenzli, R. G. Pinnick, R. L. Dod, T. Novakov, T. L. Cook, and B. D. Hinds. 1987. "Aerosol and graphitic carbon content of snow." *J. Geophys. Res.* 92: 9801–9809.

Clark, R. N., and P. G. Lucey. 1984. "Spectral properties of ice-particulate mixtures and implications for remote sensing, 1, Intimate mixtures." *J. Geophys. Res*. 89: 6341–6348.

Clarke, A. D., and K. J. Noone. 1985. "Soot in the Arctic snowpack: A cause for perturbations in radiative transfer." *Atmos. Environ*. 19: 2045–2053.

Corbett, J. J., and H. W. J. Koehler. 2003. "Updated emissions from ocean shipping." *Geophys. Res.* 108 (D20): 4650. doi:10.1029/2003JD003751.

Cuenca, R. H., M. Ek, and L. Mahrt. 1996. "Impact of soil water property parameterization on atmospheric boundary layer simulation." *J. Geophys. Res.* 101: 7269–7277.

Emori, S. 1998. "The interaction of cumulus convection with soil moisture distribution: An idealized simulation." *J. Geophys. Res.* 103: 8873–8884.

Fennessy, M. J., and J. Shukla. 1999. "Impact of initial soil wetness on seasonal atmospheric prediction." *J. Clim.* 12: 3167.

Flanner, M. G., C. S. Zender, and J. T. Randerson. 2006. "Present day climate forcing and response from black carbon in snow." *J. Geophys. Res*. In press, www.ess.uci.edu/~zender/.

Fuller, K. A., W. C. Malm, and S. M. Kreidenweis. 1999. "Effects of mixing on extinction by carbonaceous particles." *J. Geophys. Res*. 104: 15,941–15,954.

Giambelluca, T. W., D. Holscher, T. X. Bastos, R. R. Frazao, M. A. Nullet, and A. D. Ziegler. 1997. "Observations of albedo and radiation balance over postforest land surfaces in the Eastern Amazon basin." *J. Clim.* 10: 919–928.

Global Forecast System (GFS), National Center for Environmental Prediction. 2006. http://nomads.ncdc.noaa.gov/data/gfs-avn-hi/.

Goldstein, A. H., D. B. Millet, M. McKay, L. Jaegle, L. Horowitz, O. Cooper, R. Hudman, D. Jacob, S. Oltmans, and A. Clarke. 2004. "Impact of Asian emissions on observations at Trinidad Head, California, during ITCT 2K2." *J. Geophys. Res.* 109: D23S17, doi:10.1029/2003JD004406.

Grenfell, T. C., S. G. Warren, and P. C. Mullen. 1994. "Reflection of solar radiation by the Antarctic snow surface at ultraviolet, visible, and near-infrared wavelengths." *J. Geophys. Res. 99*: 18,669–18,684.

Grenfell, T. C., B. Light, and M. Sturm. 2002. "Spatial distribution and radiative effects of soot in the snow and sea ice during the SHEBA experiment." *J. Geophys. Res*. 107: 10.1029/2000JC000414.

Gribbon, P. W. F. 1979. "Cryoconite holes on Sermikavsak, West Greenland." *J. Glaciol* 22: 177–181.

Gutman, G., G. Ohring, D. Tarpley, and R. Ambroziak. 1989. "Albedo of the U.S. Great Plains as determined from NOAA-9 AVHRR data." *J. Clim.* 2: 608–617.

Hansen, J., and L. Nazarenko. 2003. "Soot climate forcing via snow and ice albedos." *Proc. Natl. Acad. Sci*. doi/10.1073/pnas.2237157100.

Hansen, J., et al. 2005. "Efficacy of climate forcing." *J. Geophys. Res.* 110: D18104, doi:10.1029/2005JD005776.

Higuchi, K., and A. Nagoshi. 1977. "Effect of particulate matter in surface snow layers on the albedo of perennial snow patches." *IAHS AISH Publ.* 118: 95–97.

Jacobson, M. Z. 1998. "Improvement of SMVGEAR II on vector and scalar machines through absolute error tolerance control." *Atmos. Environ.* 32, 791–796.

Jacobson, M. Z. 1997a. "Development and application of a new air pollution modeling system. Part II: Aerosol module structure and design." *Atmos. Environ*. 31A: 131–144.

Jacobson, M. Z. 1997b. "Development and application of a new air pollution modeling system. Part III: Aerosol-phase simulations." *Atmos. Environ*. 31A: 587–608.

Jacobson, M. Z. 1999. "Studying the effects of soil moisture on ozone, temperatures, and winds in Los Angeles." *J. Appl. Meteorol.* 38: 607–616.

Jacobson, M. Z. 2001a. "GATOR-GCMM: A global through urban scale air pollution and weather forecast model. 1. Model design and treatment of subgrid soil, vegetation, roads, rooftops, water, sea ice, and snow." *J. Geophys. Res.* 106: 5385–5402.

Jacobson, M. Z. 2001b. "GATOR-GCMM: 2. A study of day- and nighttime ozone layers aloft, ozone in national parks, and weather during the SARMAP Field Campaign." *J. Geophys. Res.* 106: 5403–5420.

Jacobson, M. Z. 2002a. "Control of fossil-fuel particulate black carbon plus organic matter, possibly the most effective method of slowing global warming." *J. Geophys. Res.* 107 (D19): 4410, doi:10.1029/ 2001JD001376.

Jacobson, M. Z. 2002b. "Analysis of aerosol interactions with numerical techniques for solving coagulation, nucleation, condensation, dissolution, and reversible chemistry among multiple size distributions." *J. Geophys. Res*. 107 (D19): 4366, doi:10.1029/ 2001JD002044.

Jacobson, M. Z. 2003. "Development of mixed-phase clouds from multiple aerosol size distributions and the effect of the clouds on aerosol removal." *J. Geophys. Res*. 108 (D8): 4245, doi:10.1029/2002JD002691.

Jacobson, M. Z. 2004. "The climate response of fossil-fuel and biofuel soot, accounting for soot's feedback to snow and sea ice albedo and emissivity. *J. Geophys. Res.* 109: D21201, doi:10.1029/2004JD004945.

Jacobson, M. Z. 2005a. "A solution to the problem of nonequilibrium acid/base gas-particle transfer at long time step." *Aerosol Sci. Technol* 39: 92–103.

Jacobson, M. Z. 2005b. "A refined method of parameterizing absorption coefficients among multiple gases simultaneously from line-by-line data." *J. Atmos. Sci.* 62: 506–517.

Jacobson, M. Z. 2005c. "Studying ocean acidification with conservative, stable numerical schemes for nonequilibrium air-ocean exchange and ocean equilibrium chemistry." *J. Geophys. Res.* 110: D07302, doi:10.1029/2004JD005220.

Jacobson, M. Z. 2005d. *Fundamentals of Atmospheric Modeling, Second Edition*. Cambridge University Press, New York. 813 pp.

Jacobson, M. Z. 2006. "Effects of absorption by soot inclusions within clouds and precipitation on global climate." *J. Phys. Chem.* 110: 6860–6873.

Jacobson, M. Z., Y. J. Kaufman, Y. Rudich. 2007. "Examining feedbacks of aerosols to urban climate with a model that treats 3-D clouds with aerosol inclusions." *J. Geophys. Res*. In review, www.stanford.edu/group/efmh/jacobson/iiie.html.

Jacobson, M. Z., and Y. J. Kaufman. 2006. "Wind reduction by aerosol particles." *Geophys. Res. Letters* 33 (24): doi:10.1029/2006GL027838.

Kahrl, W. L., ed. *The California Water Atlas*. Governor's Office of Planning and Research, Sacramento. William Kaufmann. 1979.

Ketefian G., and M. Z. Jacobson. 2007. "Development and application of a 2-D potential-enstrophy-, energy-, and mass-conserving mixed-layer ocean model with arbitrary boundaries." *Mon. Weath. Rev*. In review. www.stanford.edu/group/efmh/gsk/index.htm.

Krekov, G. M. 1993. Models of Atmospheric Aerosols. In *Aerosol Effects on Climate*. S. G. Jennings, ed. U. of Arizona Press, Tucson, Ariz., pp. 9–72.

Lanicci, J. M., T. N. Carlson, and T. T. Warner. 1987. "Sensitivity of the Great Plains severe-storm environment to soil-moisture distribution." *Mon. Wea. Rev*. 115: 2660–2673.

Light, B., H. Eicken, G. A. Maykut, and T. C. Grenfell. 1998. "The effect of included particulates on the spectral albedo of sea ice." *J. Geophys. Res*. 103: 27,739–27,752.

Liu W., P. K. Hopke, R. A. VanCuren. 2003. "Origins of fine aerosol mass in the western United States using positive matrix factorization." *J. Geophys. Res.* 108 (D23): 4716, doi:10.1029/2003JD003678.

Lobell, D. B., G. Bala, and P. B. Duffy. 2006. "Biogeophysical impacts of cropland management changes on climate." *Geophys. Res. Lett*. 33: L06708, doi:10.1029/2005GL025492.

Lu, R., and R. P. Turco. 1995. "Air pollutant transport in a coastal environment, II, Three-dimensional simulations over Los Angeles basin." *Atmos. Environ*. 29: 1499–1518.

Mahfouf, J.-F., E. Richard, and P. Mascart. 1987. "The influence of soil and vegetation on the development of mesoscale circulations." *J. Appl. Meteorol*. 26: 1483–1495.

Maricq, M., D. H. Podsiadlik, and R. E. Chase. 2000. Size distributions of motor vehicle exhaust PM: A comparison between ELPI and SMPS measurements. *Aerosol Sci. Technol* 33: 239–260.

Marticorena, B., G. Bergametti, B. Aumont, Y. Callot, C. N'Doume, and M. Legrand. 1997. "Modeling the atmospheric dust cycle. 2. Simulation of Saharan dust sources." *J. Geophys. Res*. 102: 4387.

Martien, P., and T. Umeda. 1993. Cloud cover and mesoscale surface properties derived from AVHRR satellite data to supplement SARMAP field observations in regional photochemical and modeling studies, vol. 1, in *Results and Interpretation of Field Measurements*, edited by A. J. Ranzieri and P. A. Solomon, A&WMA VIP-48, pp. 265–284, Air & Waste Manage. Assoc.

Martilli, A. 2002. "Numerical study of urban impact on boundary layer structure: Sensitivity to wind speed, urban morphology, and rural soil moisture." *J. Appl. Meteorol* 41: 1247–1266.

Mellor, G. L., and T. Yamada. 1982. "Development of a turbulence closure model for geophysical fluid problems." *Revs. of Geophys. and Space Phys*. 20: 851–875.

Miller, D. A., and R. A. White. 1998. "A conterminus United States multi-layer soil characteristics data set for regional climate and hydrology modeling." *Earth Inter. 2*.

Mintz, Y. 1984. The sensitivity of numerically simulated climates to land surface conditions. *The Global Climate*. J. Houghton, Ed., Cambridge University Press, New York, 79–105.

Moore, N., and S. Rojstaczer. 2001. "Irrigation-induced rainfall and the Great Plains." *J. Appl. Meteorol.* 40: 1297.

Mortlock, A. M., and R. Van Alstyne. 1998. Military, Charter, Unreported Domestic Traffic and General Aviation: 1976, 1984, 1992, and 2015 Emission Scenarios, NASA CR- 1998–207639. (Available at http://ntrs.nasa.gov/archive/nasa/casi.ntrs.nasa.gov/19980047346_1998120131.pdf).

National Centers for Environmental Prediction (NCEP). 2003. 2.5 degree global final analyses, distributed by the Data Support Section, National Center for Atmospheric Research.

Nijssen, B., R. Schnur, and D. P. Lettenmaier. 2001. "Global retrospective estimation of soil moisture using the variable infiltration capacity land surface model, 1980–1993." *J. Climate* 14: 1790–1808.

Noone, K. J., and A. D. Clarke. 1988. "Soot scavenging measurements in Arctic snowfall." *Atmos. Environ*. 22: 2773–2778.

Ookouchi, Y., M. Segal, R.C. Kessler, and R. P. Pielke. 1984. "Evaluation of soil moisture effects on the generation and modification of mesoscale circulations." *Mon. Wea. Rev.* 112: 2281–2292.

Park, R. J., et al. 2005. "Export efficiency of black carbon aerosol in continental outflow: Global implications." *J. Geophys. Res.* 110: D11205, doi:10.1029/2004JD005432.

Podgorny, I. A., and T. C. Grenfell. 1996. "Absorption of solar energy in a cryoconite hole." *Geophys. Res. Lett.* 23: 2465–2468.

Rind, D. 1982. "The influence of ground moisture conditions in North America on summer climate as modeled in the GISS GCM." *Mon. Wea. Rev*. 110: 1487–1494.

Roberts, G., G. Mauger, O. Hadley, and V. Ramanathan. 2006. "North American and Asian aerosols over the Eastern Pacific Ocean and their role in regulating cloud condensation nuclei." *J. Geophys. Res*. In review.

Salas, W., P. Green, S. Frolking, C. Li, and S. Boles. 2006. *Estimating irrigation water use for California agriculture: 1950s to present.* California Energy Commission, PIER Energy-Related Environmental Research, CEC-500-2006-057.

Schar, C., D. Luthi, U. Beyerle, and E. Heise. 1999. The soil-precipitation feedback: A process study with a regional climate model. *J. Clim.* 12: 722.

Segal, M., Z. Pan, R. W. Turner, and E. S. Takle. 1998. "On the potential impact of irrigated areas in North America on summer rainfall caused by large-scale systems." *J. Appl. Meteorol.* 37: 325–331.

Snyder, M. A., et al. 2006. Regional climate effects of irrigation and urbanization in the western United States: A model intercomparison. Report to the California Energy Commission Public Interest Energy Research Program. CEC-500-2006-031.

Sutkus, D. J., S. L. Baughcum, and D. P. DuBois. 2001. Scheduled Civil Aircraft Emission Inventories for 1999: Database Development and Analysis, NASA/CR-2001-211216, (available at http://gltrs.grc.nasa.gov/reports/2001/CR-2001-211216.pdf).

Toon, O. B., and T. P. Ackerman. 1981. "Algorithms for the calculation of scattering by stratified spheres." *Appl. Opt*. 20: 3657–3660.

Toon, O. B., C. P. McKay, T. P. Ackerman, and K. Santhanam. 1989. Rapid calculation of radiative heating rates and photodissociation rates in inhomogeneous multiple scattering atmospheres. *J. Geophys. Res*. 94: 16,287–16,301.

United States Environmental Protection Agency (USEPA). 2006a. Clearinghouse for Inventories and Emission Factors. www.epa.gov/ttn/chief/.

United States Environmental Protection Agency (USEPA). 2006b. AIR Data. www.epa.gov/air/data/.

United States Geological Survey United States Geological Survey (USGS) / U. Nebraska, Lincoln / European Commission's Joint Research Center 1-km resolution global landcover characteristics data base, derived from Advanced Very High Resolution Radiometer (AVHRR) data from the period April 1992 to March 1993, 1999.

VanCuren, R. A., and T. A. Cahill. 2002. "Asian Aerosols in North America: Frequency and concentration of fine dust." *Journal of Geophysical Research* 107(D24): 4804.

VanCuren R. A. 2003. "Asian aerosols in North America: Extracting the chemical composition and mass concentration of the Asian continental aerosol plume from long-term aerosol records in the western United States." *J. Geophys. Res.* 108(D20): 4623. doi:10.1029/2003JD003459.

VanCuren R. A., S. S. Cliff, K. D. Perry, M. Jimenez-Cruz. 2005. "Asian continental aerosol persistence above the marine boundary layer over the eastern North Pacific: Continuous aerosol measurements from Intercontinental Transport and Chemical Transformation 2002 (ITCT 2K2)." *J. Geophys. Res.* 110: D09S90, doi:10.1029/2004JD004973.

Walcek, C. J., and N. M. Aleksic. 1998. "A simple but accurate mass conservative, peak-preserving, mixing ratio bounded advection algorithm with FORTRAN code." *Atmos. Environ*. 32: 3863–3880.

Walker, J., and P. R. Rowntree. 1977. "The effect of soil moisture on circulation and rainfall in a tropical model." *Q. J. R. Met. Soc*. 103: 29–46.

Warren, S. G., and W. J. Wiscombe. 1980. "A model for the spectral albedo of snow. II: Snow containing atmospheric aerosols." *J. Atmos. Sci*. 37: 2734–2745.

Warren, S. G. 1982. "Optical properties of snow." *Rev. Geophys.* 20: 67–89.

Warren, S. G. 1984. "Impurities in snow: Effects on albedo and snowmelt." *Ann. Glaciol*. 5: 177–179.

Warren, S. G., and W. J. Wiscombe. 1985. "Dirty snow after nuclear war." *Nature* 313: 467–470.

Warren, S. G., and A. D. Clarke. 1990. "Soot in the atmosphere and snow surface of Antarctica." *J. Geophys. Res*. 95: 1811–1816.

Western Regional Climate Center, Western U.S. climate historical summaries. 2006. www.wrcc.dri.edu/Climsum.html.

Woo, M.-K., and M.-A. Dubreuil. 1985. "Empirical relationship between dust content and arctic snow albedo." *Cold Reg. Sci. Technol*. 10: 125–132.

Zeng, X., R. E. Dickinson, A. Walker, M. Shaikh, R. S. DeFries, and J. Qi. 2000. "Derivation and evaluation of global 1-km fractional vegetation cover data for land modeling." *J. Appl. Meteorol*. 39: 826–839.

Zhang, D., and R. A. Anthes. 1982. "A high-resolution model of the planetary boundary layer—Sensitivity tests and comparisons with SESAME-79 data." *J. Appl. Meteorol.* 21: 1594–1609.

8.0 Glossary

ALWC	aerosol liquid water content
BC	black carbon
CO	carbon monoxide
CH_4	methane
cm	centimeter
DMS	dimethyl sulfide
EPA	U.S. Environmental Protection Agency
g	gram
GHG	greenhouse gas
HNO_3	nitric acid
hPa	hectopascal
K	kelvin
NCEP	National Center for Environmental Prediction
ng/g	nanograms per gram
OM	organic matter
PIER	Public Interest Energy Research
POM	primary organic matter
RD&D	research, development, and demonstration
GATOR-GCMOM	gas, aerosol, transport, radiation, general circulation, mesoscale, and ocean model
kg	kilogram
L	liter
m	meter
mg	milligrams
mm	millimeters
m/s	meters per second
No	number?
PAN	peroxyacetyl nitrate
ppbv	parts per billion by volume
SO_2	sulfur dioxide
SOM	secondary organic matter
$\mu g/m^3$	micrograms per cubic meter
µm	micrometer
W	watts